

AD-A091 795

AIR FORCE WEAPONS LAB KIRTLAND AFB NM
NEUTRON AND GAMMA RADIATION EFFECTS ON GAALAS LASER DIODES.(U)

F/6 9/1

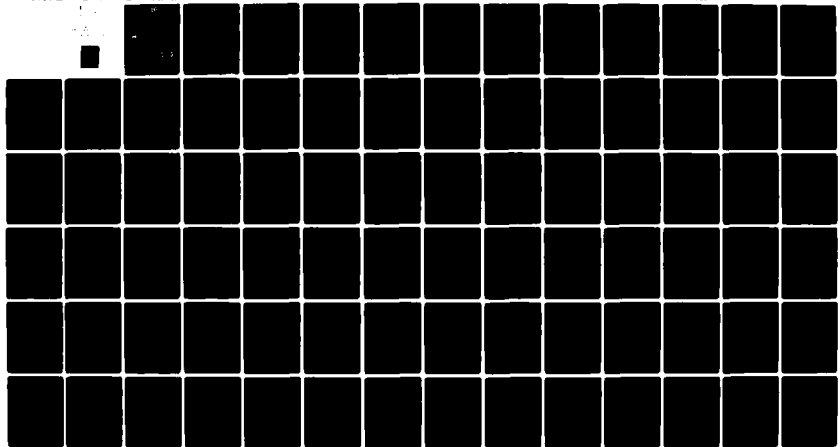
AUG 80 H ACKERMAN, T E WALSH

UNCLASSIFIED

AFWL-TR-79-43

SRTF-AD-E200 5AQ

NI

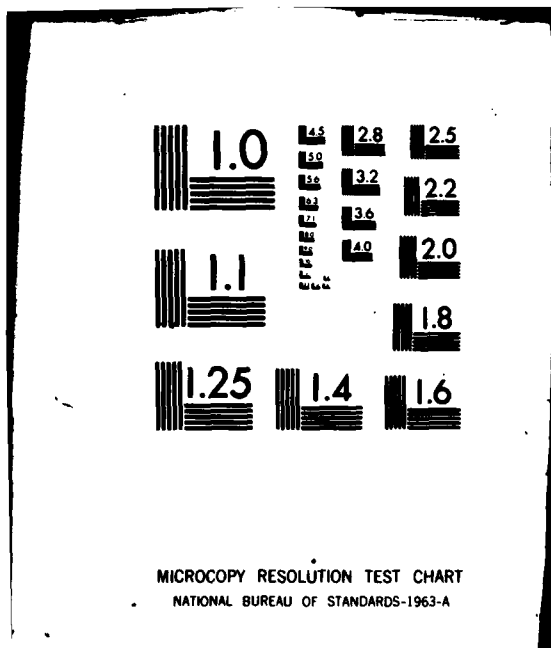


END

DATE FILMED

1-8

DTIC



AD A 091795

AFWL-TR-79-43

② LEVEL ^{III}

AP-E 200589

AFWL-TR-
79-43

NEUTRON AND GAMMA RADIATION EFFECTS
ON GaAlAs LASER DIODES

Major H. Ackerman
Capt T. E. Walsh, Jr.

August 1980



Final Report

Approved for public release; distribution unlimited.

DTIC
ELECTED
NOV 21 1980
S D
B

AIR FORCE WEAPONS LABORATORY
Air Force Systems Command
Kirtland Air Force Base, NM 87117

DDC FILE COPY

80 10 27 132

This final report was prepared by the Air Force Weapons Laboratory, Kirtland Air Force Base, New Mexico, under Job Order 88091122. First Lieutenant Marilyn McQuade (NTYC) was the Laboratory Project Officer-in-Charge.

When US Government drawings, specifications, or other data are used for any purpose other than a definitely related Government procurement operation, the Government thereby incurs no responsibility nor any obligation whatsoever, and the fact that the Government may have formulated, furnished, or in any way supplied the said drawings, specifications, or other data, is not to be regarded by implication or otherwise, as in any manner licensing the holder or any other person or corporation, or conveying any rights or permission to manufacture, use, or sell any patented invention that may in any way be related thereto.

This report has been authored by an employee of the United States Government. Accordingly, the United States Government retains a nonexclusive, royalty-free license to publish or reproduce the material contained herein, or allow others to do so, for the United States Government purposes.

This report has been reviewed by the Public Affairs Office and is releasable to the National Technical Information Service (NTIS). At NTIS, it will be available to the general public, including foreign nations.

This technical report has been reviewed and is approved for publication.

Hilmer Swenson

HILMER W. SWENSON
Capt, USAF
Project Officer

Charles A. Aeby
CHARLES A. AEBY
Actg Chief, Satellite & C³ Branch

FOR THE DIRECTOR

Norman K. Blocker
NORMAN K. BLOCKER
Colonel, USAF
Chief, Applied Physics Division

DO NOT RETURN THIS COPY. RETAIN OR DESTROY.

UNCLASSIFIED

SECURITY CLASSIFICATION OF THIS PAGE (When Data Entered)

REPORT DOCUMENTATION PAGE		READ INSTRUCTIONS BEFORE COMPLETING FORM
1. REPORT NUMBER AFWL-TR-79-43	2. GOVT ACCESSION NO. AD-A091795	3. RECIPIENT'S CATALOG NUMBER
4. TITLE (and Subtitle) NEUTRON AND GAMMA RADIATION EFFECTS ON GaAlAs LASER DIODES		5. TYPE OF REPORT & PERIOD COVERED Final Report
		6. PERFORMING ORG. REPORT NUMBER
7. AUTHOR(s) Maj Harro Ackerman Capt Thomas E. Walsh, Jr	8. CONTRACT OR GRANT NUMBER(s)	
9. PERFORMING ORGANIZATION NAME AND ADDRESS Air Force Weapons Laboratory (NTYC) Kirtland Air Force Base, NM 87117		10. PROGRAM ELEMENT, PROJECT, TASK AREA & WORK UNIT NUMBERS 62601F/88091122
11. CONTROLLING OFFICE NAME AND ADDRESS Air Force Weapons Laboratory (NTYC) Kirtland Air Force Base, NM 87117		12. REPORT DATE August 1980
		13. NUMBER OF PAGES 80
14. MONITORING AGENCY NAME & ADDRESS (if different from Controlling Office)		15. SECURITY CLASS. (of this report) Unclassified
		15a. DECLASSIFICATION/DOWNGRADING SCHEDULE
16. DISTRIBUTION STATEMENT (of this Report) Approved for public release; distribution unlimited.		
17. DISTRIBUTION STATEMENT (of the abstract entered in Block 20, if different from Report)		
18. SUPPLEMENTARY NOTES		
19. KEY WORDS (Continue on reverse side if necessary and identify by block number) Laser Diodes Threshold Current GaAlAs Quantum Efficiency Neutron Radiation Damage Factors Gamma Radiation Damage Constants Radiation Effects		
20. ABSTRACT (Continue on reverse side if necessary and identify by block number) The effects of two kinds of radiation on the performance of double heterojunction aluminum-gallium-arsenide (AlGaAs) laser diodes were investigated. One set of diodes received neutron radiation in a nuclear reactor; another set was exposed to gamma radiation from a cobalt-60 (Co^{60}) source. Each set contained two types of lasers, an RCA C30127 and a Laser Diode Laboratories LCH-10, both designed to operate continuously at room temperature. At neutron fluences of 10^{14} n/cm ² , both types of diodes showed significant decreases in power output and external quantum efficiency, and increases in threshold current. There was no (over)		

DD FORM 1 JAN 73 1473

UNCLASSIFIED

SECURITY CLASSIFICATION OF THIS PAGE (When Data Entered)

UNCLASSIFIED

SECURITY CLASSIFICATION OF THIS PAGE(When Data Entered)

20. ABSTRACT

significant change in bias voltage versus forward current or in spectral composition of the light outputs at neutron fluences up to 10^{15} n/cm². Under gamma radiation, the C30127 laser exhibited rapid degradation. A dosage of 10^4 rad(Si) reduced the output power by half. Threshold current, efficiency, and intensity distribution were all adversely affected. The damage factor at constant voltage was 1.5×10^{-7} rad⁻¹. The LCW-10 performance improved to a dosage of 10^6 rad(Si) before degradation began. After 10^8 rad(Si), power output was still comparable to preirradiation values. Beam characteristics were not appreciably altered. The damage factor at constant voltage was 4×10^{-8} rad⁻¹.

UNCLASSIFIED

SECURITY CLASSIFICATION OF THIS PAGE(When Data Entered)

CONTENTS

<u>Section</u>		<u>Page</u>
I	INTRODUCTION	5
II	THEORY OF OPERATION AND NEUTRON DAMAGE EFFECTS	8
III	EXPERIMENTAL EQUIPMENT AND PROCEDURES	19
IV	RESULTS	24
V	DISCUSSION AND RECOMMENDATIONS	36
VI	GAMMA RADIATION-INDUCED EFFECTS	40
VII	DESCRIPTION OF SAMPLES AND EXPERIMENTS - GAMMA IRRADIATION WORK	46
VIII	RESULTS AND DISCUSSION	50
IX	CONCLUSIONS	76
X	RECOMMENDATIONS	77

Accession For	
NTIS GRA&I	<input checked="" type="checkbox"/>
DTIC TAB	<input type="checkbox"/>
Unannounced	<input type="checkbox"/>
Justification	
By _____	
Distribution/ _____	
Availability Codes	
Dist	Avail and/or Special
A	

ILLUSTRATIONS

<u>Figure</u>		<u>Page</u>
1	Stripe geometry laser diode	6
2	Cross-section of laser package	9
3	Front view of typical stripe geometry AlGaAs injection laser	9
4	Energy band diagram for a heavily doped p-n junction	10
5	Density-of-states for laser diode	11
6	Apparatus for measuring power output	22
7	Circuit for measuring power and voltage	23
8	Power versus current of RCA No. 550 at several fluences	26
9	Increase in threshold current versus neutron fluence	27
10	Power versus $(I - I_{th})$ for RCA Diode No. 65	29
11	Change in differential quantum efficiency versus neutron fluence	30
12	Relative power output at 100 mA above threshold versus neutron fluence	31
13	Relative power output at 200 mA versus neutron fluence	33
14	Bias voltage versus forward current	34
15	Estimated increase in threshold current versus neutron fluence	37
16	Circuit for measuring I-V, P-V relationships	47
17	Configuration for obtaining spectral data	48
18	Shift of emission peak with applied voltage at 77 K, preirradiation	
	a. Sample 1	52
	b. Sample 2	52
19	Shift of emission peak with applied voltage at 77 K, preirradiation	
	a. Sample 66	53
	b. Sample 68	53
20	Preirradiation power-voltage and current-voltage relation at 77 K	
	a. Samples 1 and 2	54
	b. Samples 66 and 68	54

ILLUSTRATIONS (CONTINUED)

<u>Figure</u>		<u>Page</u>
21	Preirradiation power efficiency at 77 K	55
	a. Samples 1 and 2	55
	b. Samples 66 and 68	55
22	Power-current relation as function of dosage at 77 K	56
	a. Sample 1	56
	b. Sample 2	56
	c. Sample 66	57
	d. Sample 68	57
23	Power-voltage and current-voltage relation at 77 K, pre- and postirradiation (sample 1)	61
24	Power-voltage and current-voltage relation at 77 K, pre- and postirradiation (sample 2)	62
25	Power-voltage and current-voltage relation at 77 K, pre- and postirradiation (sample 66)	63
26	Power-voltage and current-voltage relation at 77 K, pre- and postirradiation (sample 68)	64
27	Constant voltage and constant current change in power output at 77 K	
	a. Sample 1	65
	b. Sample 2	65
	c. Sample 66	66
	d. Sample 68	66
28	Power efficiency at 77 K for selected dosages	
	a. Sample 1	69
	b. Sample 2	69
	c. Sample 66	70
	d. Sample 68	70
29	Intensity distribution in far field, pre- and post- irradiation (sample 1)	
	a. Parallel to junction	71
	b. Perpendicular to junction	71
30	Intensity distribution in far field, pre- and post- irradiation (sample 2)	
	a. Parallel to junction	72
	b. Perpendicular to junction	72

ILLUSTRATIONS (CONTINUED)

<u>Figure</u>		<u>Page</u>
31	Intensity distribution in far field, pre- and post-irradiation	
	a. Parallel to junction	73
	b. Perpendicular to junction	73
32	Intensity distribution in far field, pre- and post-irradiation (sample 68)	
	a. Parallel to junction	74
	b. Perpendicular to junction	74

TABLES

<u>Table</u>		<u>Page</u>
1	Threshold current damage factors	28
2	Differential quantum efficiency damage factors	31
3	Power damage factors	32
4	Typical operating characteristics at room temperature as provided by manufacturer	46
5	Specific information provided by manufacturer	46
6	Measured preirradiation characteristics at room temperature	50
7	Measured preirradiation characteristics at 77 K	51
8	Threshold current as function of dosage	58
9	Postirradiation power output at specific forward currents	58
10	Calculated damage factors, $\tau_0 K$	67
11	Emission peak measured at constant current as a function of dosage	75
12	Beam divergence before and after irradiation	75

I. INTRODUCTION

Some proposed applications of injection lasers require their operation in a nuclear radiation environment. It is, therefore, necessary to know the effects of radiation on laser performance. Radiation damage studies provide this knowledge and also give some insight into the physical processes occurring in the devices.

Since the development of the first laser diodes over 15 years ago, many advances have been made toward understanding and optimizing their performance. The lasers developed have the advantage of small size, and since they convert electrical power directly into coherent light, the output can be modulated simply by modulating the input current (Ref. 1). Until recently, however, these devices could not be operated continuously at room temperature, making them impractical for many applications.

The development of continuous-wave (CW) laser diodes which operate at room temperature has resulted in improvement in the efficiency and quality of the devices. Gallium-arsenide (GaAs) and some other three- to five-compound semiconductors are used for the devices because they have a direct gap between the conduction band and the valence band. This means that no momentum change is required in the band-to-band transition, and radiative transitions may occur with the emission of only a photon. Consequently, much higher gain can be achieved for the same pumping level (Ref. 2).

The first laser diodes were made by diffusing an acceptor into a heavily doped n-type substrate, forming a p-n junction. The thickness of the recombination region was kept to a minimum by introducing a steep doping profile. An even thinner active region was made by depositing p-type material onto the substrate with a process called vapor phase epitaxy and later with liquid phase epitaxy (LPE). It was then found that aluminum could be substituted for gallium in some of the lattice sites of GaAs to raise the band gap and decrease the index of refraction. A layer of degenerately doped p⁺ aluminum-gallium (AlGa) was deposited on a thin p-layer to form a single heterojunction (SH) laser. Because of the decrease in index of refraction in the p⁺ region, the active region was better confined and there was less optical loss outside the cavity.

Later, double heterojunctions were used to confine the active region even further and to give more precise control of its thickness. Additionally, the

use of aluminum-gallium-arsenide (AlGaAs) in the active region allows the wavelength of the emitted light to be controlled somewhat by varying the ratio of aluminum to gallium, thus varying the band-gap energy.

Even with active regions only a few μm thick, the diodes still could not dissipate enough heat to be operated continuously at room temperature. Room temperature operation was achieved by confining the active region laterally. Instead of injecting carriers along the entire width of the junction, the injection current was confined to the center of the junction by a narrow stripe contact on the p^+ region as illustrated in Figure 1. Limiting the volume of the active region in this way allowed the volume of the crystal to accept the heat generated in the active region. The stripe geometry also reduced the threshold current (I_{th}) for laser operation (Ref. 3).

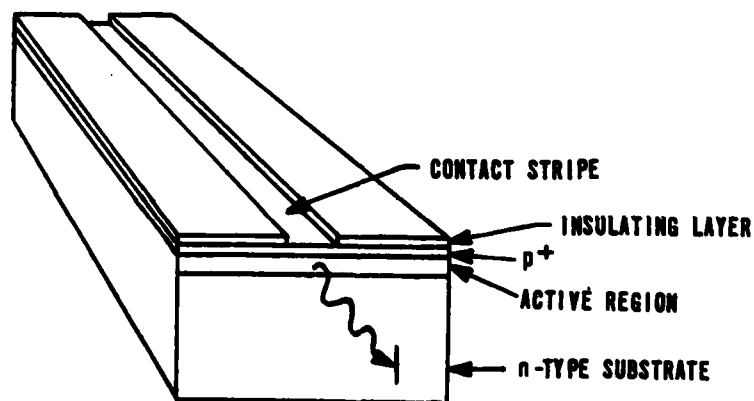


Figure 1. Stripe geometry laser diode.

Several studies have investigated the effects of various types of radiation on GaAs compounds and on pulsed GaAs lasers. These studies examined the optical properties and electrical behavior of a GaAs p-n junction (Ref. 4) or the effect of irradiation on operation of GaAs lasers at or below threshold (Ref. 5). Southward, et al (Ref. 6), did extensive work on such lasers operating above threshold.

The Southward study dealt with fast neutron damage of diffused GaAs injection lasers. The report discussed an increase in threshold current with irradiation, a reduction in power output above I_{th} , and an increase in the delay associated with modulation of the diodes, as well as the effects of temperature variation on these quantities.

Saji and Inuishi (Ref. 7), working with pulsed GaAs lasers at liquid nitrogen temperature, noticed that after exposing the sample to cobalt-60 (Co^{60}), efficiency decreased, threshold current increased, and the emission peaks shifted. They postulated that the increase in I_{th} was caused by indirect recombination centers associated with the radiation induced defects. Other investigators attributed the increase in I_{th} to a decrease in the electroluminescent efficiency or to an increased optical absorption in the active region (Ref. 8). The decrease in output and efficiency is attributed to the introduction of nonradiative recombination centers which compete with radiative centers for the excess carriers injected. The effect of these centers is to decrease both the nonradiative lifetime and the total carrier lifetime (Ref. 9).

Reference 10 finds these explanations insufficient to account for the exponential decrease in efficiency which were observed, and introduced the concept of the luminescent killer center to explain the results. It was suggested that defects were introduced that quenched the radiative recombination process in a volume extending over several radiative recombination centers.

In this work, two sets of AlGaAs lasers were tested. One set was subjected to neutron radiation in a nuclear reactor, the other to gamma radiation from a Co^{60} source. Each set contained two types of CW, room-temperature laser diodes: C30127, manufactured by RCA, and LCW-10 manufactured by Laser Diode Laboratories, Inc.

This report is divided into two main parts. The first part discusses the neutron irradiation work and comprises Section II through V. Section II presents the theory of laser diode operation and a model for the neutron degradation of the devices. Section III describes the experimental equipment and procedures, and the results of the experiments are given in Section IV. Section V contains a discussion of the significance of the results and recommendations for further research.

The second part (Sections VI through X) concerns the gamma irradiation work. Specific gamma-induced effects are discussed in Section VI, the individual measurements in Section VII, and the experimental results in Section VIII. Section IX summarizes the findings of the gamma irradiation investigation and Section X presents suggestions for additional work.

II. THEORY OF OPERATION AND NEUTRON DAMAGE EFFECTS

OPERATION OF INJECTION LASERS

There are three requirements for the operation of an injection laser. First, a medium in which stimulated emission will occur is needed so that optical gain can be produced. Next, there must be a cavity with partially reflecting ends that will cause the light to pass through the medium until sufficient intensity is achieved. Finally, there must be some method of pumping the medium to achieve a population inversion.

In semiconductor materials transitions such as absorption, spontaneous emission, and stimulated emission occur between energy bands instead of between discrete energy levels. The band gaps in semiconductors may be divided into two categories, direct and indirect. Electron transitions across a direct band gap do not require a change in momentum; therefore, the transition may occur with the emission of only a photon. It is in direct band gap materials that stimulated emissions may occur readily and lasing has been observed.

The application of a forward bias to a semiconductor laser creates a narrow region containing both holes and electrons. Recombination occurs within this region with the emission of radiation. The condition for spontaneous emission has thus been created. Amplification occurs if radiation of energy near the band gap energy travels through the region and stimulates the transition and if the population inversion is maintained by the injection of carriers.

A resonant cavity for the radiation is normally created by constructing the injection laser in the form of a Fabry-Perot cavity; i.e., with parallel reflecting surfaces normal to the active region. Low injection current results in spontaneous emission and, as the current is increased, a point is reached where gains exceed losses and lasing action begins. This is expressed by

$$g = \alpha + 1/L \ln \left(1/(R_1 R_2) \right)^{1/2} \quad (1)$$

where

g = the gain per unit length

α = losses per unit length

L = the length of the cavity

R_1 & R_2 = reflectives of the end surfaces

Maximum gain occurs in the junction region where the population inversion exists, and radiation traveling through the device is confined to this region by changes in the dielectric constant and, hence, in the refractive index of the material.

The injection lasers used in this investigation were stripe geometry, double-heterojunction devices, and were packaged as shown in Figure 2.

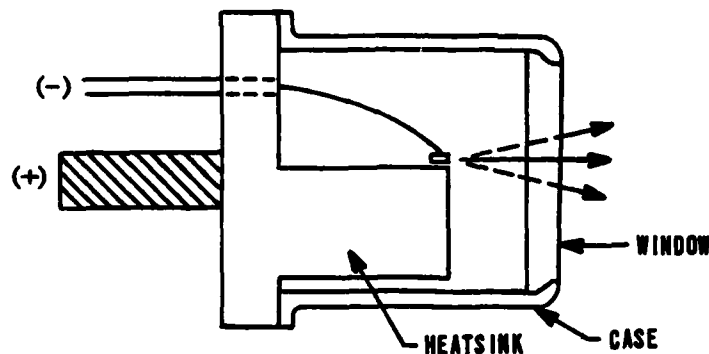


Figure 2. Cross-section of laser package.

A typical stripe geometry AlGaAs laser may be constructed as illustrated in Figure 3. The layers of a specific laser may be arranged differently, possibly including other layers as buffers or to assist in optical confinement.

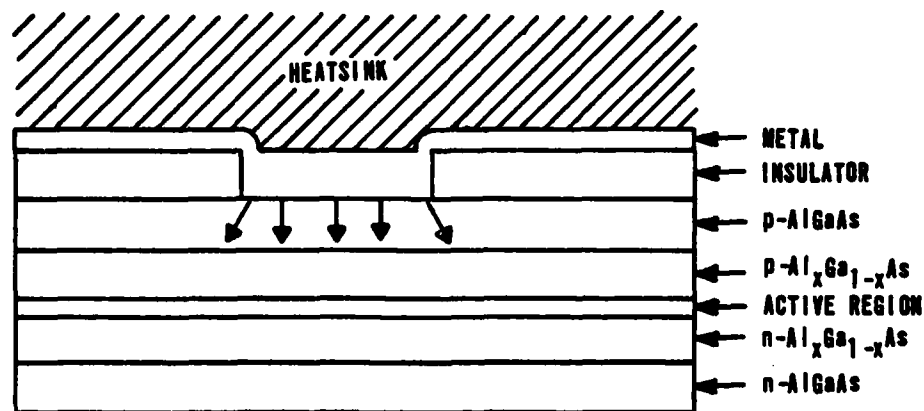


Figure 3. Front view of typical stripe geometry AlGaAs injection laser.

The injection current is confined to a narrow region, as indicated by the arrows, emanating from the metallic stripe shown in Figure 3. Recombination occurs in the narrow active region and light is emitted in a fan-shaped beam from one of the polished end surfaces.

Band-to-band transitions occur when electrons in the conduction band combine with holes in the valence band (Figure 4). This transition may result in a photon emission (radiative transition) or a phonon or free electron emission (nonradiative transition). Generally, laser diodes are doped with a high density of donors. The donor material on the p-side causes a tail of states below the conduction band. Because the energy of emitted photons is generally less than the band gap, it is thought that the lasing transition occurs between the conduction band tail and the impurity level just above the valence band as depicted in Figure 5 (Ref. 11).

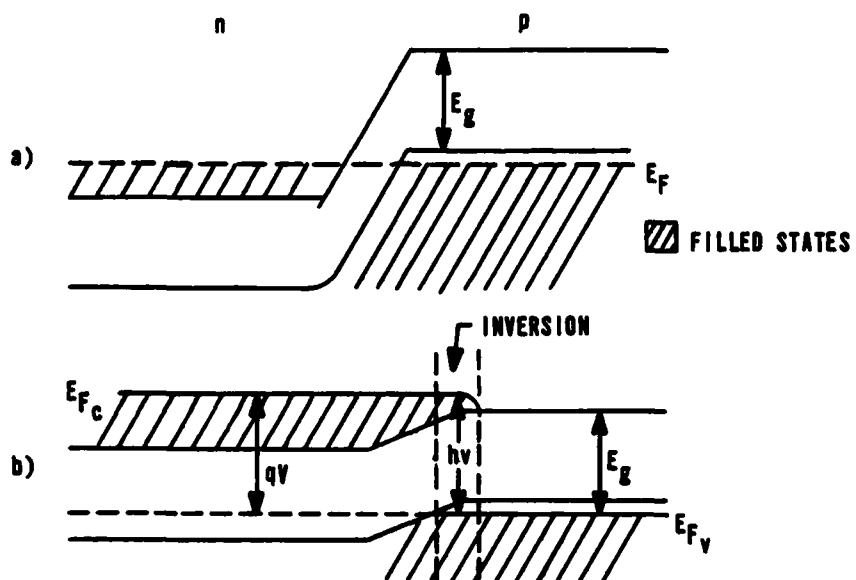


Figure 4. Energy band diagram for a heavily doped p-n junction.

The fact that the emission peak of a GaAs laser shifts as the applied voltage is increased implies that a tunneling mechanism is also involved in the lasing transition. Photon assisted tunneling may occur when sufficient forward bias is applied to the junction to uncross the bands. An electron can tunnel through the energy barrier between the conduction band of the n-material into the forbidden region of the p-material. It then drops into an empty valence band or impurity level state, and a photon is emitted. The energy of the photon emitted by this process is a function of the applied voltage. This accounts for the observed shift in the emission wavelength with applied energy as shown in Reference 6.

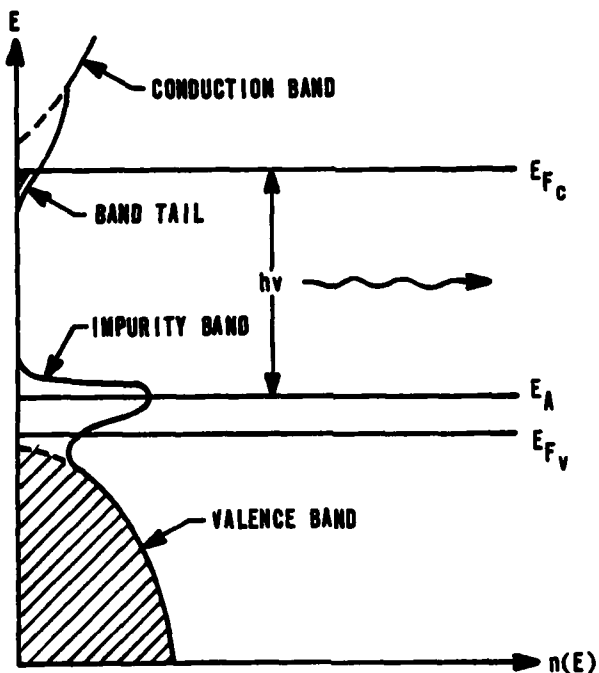


Figure 5. Density-of-states for laser diode.

Although the band-to-acceptor and photon-assisted tunneling transitions are not the only possible radiative transitions, they are generally considered to be the most likely candidates for the majority of radiative processes in a GaAs laser diode. In addition to radiative transitions, there are many nonradiative transitions that may occur in a laser diode. The same transitions that result in the emission of a photon may also occur with the emission of other energy conserving particles, such as phonons or free electrons. The most significant nonradiative recombination processes are those that involve deep energy levels. Transitions due to tunneling to deep levels or between the band and deep levels are nonradiative processes and have been associated with crystal lattice dislocations in GaAs laser diodes (Ref. 12).

During laser operation, both radiative and nonradiative transitions occur. The ratio of the radiative recombinations to the total number of transitions is called the internal quantum efficiency (n_i):

$$n_i = \frac{\text{No. of radiative recombinations (photons emitted)}}{(\text{No. of radiative recombinations} + \text{No. of nonradiative recombinations})} \quad (2)$$

This quantity, although difficult to measure, is useful in describing the operation of a laser, particularly in relating the current density (J) to the optical gain (g). Internal quantum efficiencies approaching 100 percent have been observed in GaAs laser diodes at low temperatures. Values for room temperature operation are about 50 percent as shown in Reference 11.

For a laser to operate, the optical gain per unit length must at least equal the losses in the cavity. The losses consist of absorptions per unit length (α) and losses through the ends with reflectivity R . The decrease in intensity (I) of light traveling through the cavity is given by Reference 13.

$$dI = -\alpha I dx + g I dx \quad (3)$$

where g is the optical gain per unit length. A fraction of light R will be lost at each end of the cavity.

Integration of net loss (or gain) over a complete round trip through a cavity with length L gives the expression

$$I = I_0 R^2 e^{2gL-2\alpha L} \quad (4)$$

The threshold gain (g_{th}) is obtained by substituting the relationship $I = I_0$ and solving for g to give the relation

$$g_{th} = \alpha + 1/L \ln 1/R \quad (5)$$

The relationship between gain and current density is

$$g = c^2 n_f J^b / 8 \pi q n^2 v^2 \Delta v d \quad (6)$$

where

c = speed of light in a vacuum

q = electronic charge

n = the material index of refraction

v = the frequency of the light emitted

Δv = the recombination line width

The exponent b is equal to unity for a simple two-level system. In a real semiconductor, the value of b depends on the density of states distribution. No experimental value of b has been found, so for the purposes of this paper, it will be considered to be unity.

Equation 6 may be rewritten as

$$g = \beta J \quad (7)$$

where β is called the gain constant. This expression may be substituted into Equation 5 to give the relationship for threshold current density.

$$J_{th} = 1/\beta (\alpha + 1/L \ln 1/R) \quad (8)$$

It should be noted that the term α includes absorption in the regions adjoining the cavity as well as those occurring in the cavity. Each region in a double-heterojunction laser diode has a different absorption coefficient. The term α appearing in Equation 8 incorporates α_1 , α_2 , and α_3 for each of the three regions along with functions determined by the waveguide geometry.

As mentioned earlier, the internal quantum efficiency of a laser diode is difficult to determine. For this reason, a quantity called external quantum efficiency (n_{ext}) has been defined. Just as internal quantum efficiency is a measure of the percentage of radiative transitions inside the diode, the external quantum efficiency is a measure of the percentage of photons emitted by a laser diode with respect to the number of electrons passing through it.

$$n_{ext} = \text{No. of photons emitted}/\text{No. of electrons passing through device} \quad (9)$$

$$= \frac{P/h\nu}{I/q} = \frac{P}{IV_j} \quad (10)$$

where

P = output power of the device

I = the bias current

V_j = the junction voltage

Below threshold, the emission from a laser diode is primarily spontaneous, and n_{ext} is small. Above threshold, the stimulated emissions quickly render the spontaneous emission insignificant and n_{ext} ideally increases linearly with increasing current. The slope of the increasing P versus I curve is known as the differential quantum efficiency (Δn).

$$\Delta n = \Delta P/V_j \Delta I \quad (11)$$

If n_{ext} is considered for only stimulated emission, then

$$\Delta n = \frac{(P - P_{th})}{(I - I_{th}) V_i} = \frac{P}{(I - I_{th}) V_i} \quad (12)$$

Using assumptions stated before, one can show that

$$\Delta n = n_i \frac{1/L \ln 1/R}{\alpha + 1/L \ln 1/R} \quad (13)$$

Thus, the differential quantum efficiency is proportional to internal quantum efficiency and inversely proportional to the absorptions in the device.

CURRENT FLOW IN THE INJECTION LASER

The total current flowing across a p-n junction in an injection laser consists of two components. One component, due to a diffusion process, results from carriers surmounting the barrier and recombining on the other side of the junction. The other, due to space charge region (SCR) recombination, results from carriers entering the depletion region and recombining there. The light output of the laser may be due to radiative recombinations resulting from one or the other of the components, or to a combination of both. That portion of the total current which results in radiative transitions is referred to as the radiative current.

The expression for the diffusion current is

$$I_D = \frac{qAD^{1/2} n_{po}}{\pi^{1/2}} \exp \frac{qV}{kT} \quad (14)$$

where

- q = the electronic charge
- A = the junction area
- D = the electron diffusion coefficient
- n_{po} = the minority carrier density
- τ = the carrier lifetime
- V = the applied voltage
- k = Boltzmann's constant
- T = the temperature

The SCR current is given by

$$I_{SCR} = \frac{qn_i wA}{2\tau} \exp \frac{qV}{2kT} \quad (15)$$

where

n_i = the intrinsic carrier density
 w = the width of the space charge region

The total current flow is normally due to a combination of the two mechanisms, but since SCR current increases faster than diffusion current as the energy gap widens, the total current is normally given as $I_{tot} \approx I_{SCR}$ for comparatively large gap materials such as GaAs.

RADIATION DAMAGE TO LASER DIODES

Neutron irradiation of a GaAs crystal may cause damage to the crystal by any of several mechanisms. If a fast neutron interacts with the crystal, it might knock atoms from the lattice, thereby leaving a vacancy. Additionally, the atom that was removed may be deposited interstitially. If the neutron energy is large enough, it can transfer enough energy to the displaced atom to set up an avalanche of vacancies and interstitials. This would leave a relatively large damaged area within the crystal. Neutrons interacting with the crystal may also transmute some atoms by neutron absorption reactions which would create additional impurities. A final possibility is ionization of lattice atoms, thereby creating additional charge carriers.

Two of the effects of neutrons, ionization and transmutation, are insignificant in their effect on laser diode operation. The high level of impurity doping (about $10^{18}/\text{cm}^3$) overpowers the small amount of impurities that would be produced by neutron activation (upper estimate is about $5 \times 10^{14}/\text{cm}^3$ in this experiment). Ionizations are not significant because the free electrons quickly recombine with ionized centers until equilibrium is again reached.

Lattice damage in the form of displacements, interstitials, and dangling bonds is significant in its effect on laser diode operation. These defects cause local perturbations in the energy levels and form additional recombination centers. If these are nonradiative recombination centers, the internal quantum efficiency of the device will probably decrease. If the centers give radiative recombinations, then there may be radiation produced at a new wavelength because of the displaced energy levels in the region of the damage. Other possible effects of lattice damage include changes in index of refraction, increased absorption or scattering, and changes in electrical properties such as carrier lifetime, electrical resistance, and carrier mobility.

Early studies of radiation effects in GaAs were performed by Aukerman and others to determine changes in electrical and optical properties of the material (Ref. 4). They found that the conductivity of GaAs decreased significantly after exposure to a large fluence of neutrons (10^{16} n/cm²). They also found an increase in absorption band edge with moderate (10^{16} n/cm²) irradiation. Another result of this study was the discovery of additional energy levels in GaAs after irradiation.

In addition to the mechanisms of physical damage described before, Aukerman (Ref. 4) referenced a phase change reaction proposed by Edwards and others. A fast neutron may deposit enough energy in a small volume of the crystal to create a pocket of high temperature and pressure. This will cause the material to change irreversibly to a metallic phase, creating a relatively large perturbation in the energy levels of the semiconductor in that region.

More recent studies by Barnes (Refs. 5 and 14) dealt with neutron damage in close confinement (referring to the active region confinement) GaAs laser diodes at and below threshold. He found, by using diodes with cavities of different lengths, that the primary mechanism for increases in threshold current after irradiation was a decrease in internal quantum efficiency. In his study, little increase in the absorption coefficient was indicated.

The basic model for damage used by Barnes (and later Southward) is that the neutron fluence causes a linear increase in the reciprocal of the lifetime (τ) of the carriers:

$$\frac{1}{\tau} = \frac{1}{\tau_0} + K \phi \quad (16)$$

or

$$\tau_0 / \tau(\phi) - 1 = \tau K \phi \quad (17)$$

where

τ_0 = the unirradiated lifetime

K = a damage constant

ϕ = the neutron fluence

The radiative lifetime is a measure of the probability of a radiative recombination occurring, and the nonradiative lifetime is a measure of the probability of a nonradiative recombination occurring (recombination rate is proportional to $1/\tau$). Thus, the internal quantum efficiency can be expressed in terms of τ :

$$\eta_i = \frac{\text{total lifetime}}{\text{radiative lifetime}} = \frac{\tau}{\tau_R} \quad (18)$$

The centers formed by neutron irradiation may be either radiative or non-radiative. From the preceding discussion and from the results of previous studies, it is evident that more nonradiative centers are formed and the η_i decreases. If the decrease in radiative lifetime is much less than the decrease in total lifetime, τ_R in Equation 18 can be considered to be constant in the presence of a neutron flux. Therefore, Equation 18 can be substituted into Equation 17 to give the relationship for neutron degradation of internal quantum efficiency.

$$\eta_i(0)/\eta_i(\phi) - 1 = \tau_0 K_{ni} \phi \quad (19)$$

where K_{ni} is the damage constant for internal quantum efficiency.

Expressions for the changes in threshold current and differential quantum efficiency may be derived using Equation 19. Since Barnes found that the degradation was due to a decrease in η_i and not an increase in α , all the terms in Equation 8 except β may be considered to be constant with respect to an increase in neutron fluence. Therefore, as β is directly proportional to η_i , making I_{th} inversely proportional, the expression for the increase in threshold current may be written:

$$I_{th}(\phi)/I_{th}(0) - 1 = \tau_0 K_I \phi \quad (20)$$

where K_I is the damage constant for threshold current. From Equation 13 it is seen that Δn is directly proportional to n giving

$$\Delta n(0)/\Delta n(\phi) - 1 = \tau_0 K_\Delta \phi \quad (21)$$

where K_Δ is the Δn damage constant.

Combining Equations 12 and 21 gives the relationship for power reduction at a constant current above threshold; i.e., $I - I_{th} = \text{constant}$.

$$P(0)/P(\phi) - 1 = \tau_0 K_p \phi \quad (22)$$

where K_p is the power damage constant.

The model for radiation damage presented here is very simple. The basic assumption is that radiative lifetime increases linearly with respect to total

lifetime when the material is exposed to a flux of fast neutrons. This results in a linear increase in threshold current and a linear decrease in power at a constant current above threshold. Although the model is simple, it has been used successfully to explain results in other studies such as those of Southward and Barnes.

III. EXPERIMENTAL EQUIPMENT AND PROCEDURES

LASER DIODES

The devices used for this study were manufactured by RCA and Laser Diode Laboratories, Inc., and supplied by the Air Force Weapons Laboratory. Both types of diodes are designed for continuous infrared (IR) emission at room temperature. In both types the heterostructure is grown by liquid phase epitaxy, and both use a stripe contact to limit the width of the active region. Although much information about the construction of the diodes is proprietary, some of the main differences can be presented.

The RCA C30127 laser diode consists of probably four regions (Ref. 12) with an oxide-isolation stripe contact. The active region of n-type $\text{Al}_y\text{Ga}_{1-y}\text{As}$ is sandwiched between two layers of $\text{Al}_x\text{Ga}_{1-x}\text{As}$, one p-type and one n. The value of y (probably about 0.1) is smaller than the value of x (probably about 0.3) so that the band gap in the recombination region is less than that in the adjoining regions. A highly doped p-type GaAs layer is grown next to the p-type AlGaAs layer to provide a better ohmic contact with the metallic stripe.

In the RCA diode, the contact stripe is formed by depositing a layer of insulating SiO_2 on the surface of the p⁺ region. A 13 μm wide stripe is removed along the desired active area. The individual devices are made from the wafer by cleaving the wafer into slivers and sawing the slivers into sections. The cleaved ends of the device form the reflecting surfaces of a Fabry-Perot lasing cavity. The sawed edges have low reflectivity, thus suppressing horizontal modes in the cavity.

After the individual diodes are formed the laser is passivated, that is, the end facets of the laser are coated with a dielectric material to reduce the possibility of catastrophic degradation due to facet damage. The p-side of the device is then indium-soldered to a copper heatsink with the SiO_2 insulating all but the stripe region.

The Laser Diode Laboratories LCW-10 is manufactured in much the same way but with a few important differences. The aluminum concentration in the active region is slightly lower than that for RCA diodes, resulting in a shorter wavelength of emission. This region is also p-type rather than n-type as in the RCA devices. The sandwich layers contain a slightly higher concentration of aluminum ($x = 0.35$) than the RCA diodes which may give better confinement of the

active region. Also, there are two additional layers in the LCW-10 diode, both n-type. The substrate is grown with a very low dislocation density ($1000/\text{cm}^2$) by the gradient-freeze technique. Onto this layer is grown a layer of n-type GaAs designed to terminate dislocation networks or substrate surface imperfections. These two layers greatly reduce the possibility of gradual degradation of the device caused by dislocation migration into the active region (Ref. 15).

Additional precaution against defect formation is taken by using a monolithic stripe. Instead of etching a stripe in a deposited layer of an oxide insulator, a layer of n-type GaAs is deposited and then etched to form a 15-micron wide stripe. This n-layer forms a reverse biased p-n junction which is nonconducting except in the stripe region where the n-type material has been removed. This method is simple, it reduces the danger of forming lattice defects near the surface of the pellet, and reduces the stress on the surface of the chip. Additionally, thermal conduction from the laser to the heatsink is better because of the absence of the oxide layer, which is a poor thermal conductor (Ref. 15).

IRRADIATION FACILITIES AND PROCEDURES

The source of neutrons used for irradiation of the laser diode samples was the Ohio State University nuclear reactor. It is a swimming pool reactor with a maximum power level of 10 kW. The core of the reactor consists of a 5-by-5 array of 20 fuel elements, 4 control rod elements, and a central irradiation facility (CIF). The fuel elements are standard 10-plate elements of uranium-aluminum alloy clad with aluminum. The enrichment is 93 percent U-235 (Ref. 16).

Irradiations for this experiment were performed in the CIF of the reactor. This facility is a 1-1/2 inch diameter aluminum pipe located in the core at matrix position (3,3). The inside of the pipe is dry and samples may be lowered by string to the geometric center of the core. The unperturbed neutron flux in the CIF with the reactor operating at 10 kW is $3.97 \times 10^{11} \text{ n/cm}^2\text{-s}$, of which 50 percent are thermal neutrons (E less than $4.75 \times 10^{-7} \text{ MeV}$), 50 percent are epithermal neutrons (E greater than $4.75 \times 10^{-7} \text{ MeV}$), and 21 percent are fast neutrons (E greater than 0.5 MeV) (Ref Ohio State Handout on reactor fluxes). About 5 percent of the total dose at 10 kW is due to gamma radiation. This is a dose of about $6 \times 10^5 \text{ rad/hr}$, which is much less than the gamma dose given to the diodes in the work described later in this report.

For this experiment, each sample was irradiated inside a 2-inch by 3/4-inch cylindrical plastic vial lined with a 0.040-inch thick coating of cadmium to absorb thermal neutrons. The liner consisted of a disc in the bottom of the vial, a 1-inch high cylinder, and a removable top. Since the end caps were not formed to overlap the cylinder, the liner was inspected visually before each irradiation to assure that there were no gaps.

The sample was placed inside the liner along with a nickel wire for monitoring the flux. No attempt was made to position the wire or the laser diode at a certain spot inside the liner. After the sample and wire were in place, the plastic vial was put in a basket and lowered by string into the core. A knot in the string was used to mark the distance from the top of the CIF pipe to the center of the core. Timing for the irradiation began when the sample arrived at the core center if the reactor was already at full power when the sample was inserted, or, if the sample was inserted before reactor startup, when full power (10 kW) was reached. Timing was ended when the sample was removed from the core or when the reactor was shut down.

After the vial was removed from the reactor, the sample was removed and monitored for gamma and beta activity before its operating characteristics were tested. The flux monitoring wire was analyzed with a GeLi detector and a Canberra 4096 channel analyzer. A minicomputer program gave the activity of the cobalt-58 (Co^{58}) directly from the data in the analyzer. The 810 keV photo-peak of Co^{58} was used to determine the activity of the wire.

Two diodes were irradiated at liquid nitrogen temperature. For this experiment, a cadmium liner was placed inside a polystyrene container. After the diode and flux wire were in place, the container was filled with liquid nitrogen and lowered into the CIF. After five minutes of irradiation, the container was removed and the diode was dumped into a cup of liquid nitrogen and carried to the experimental area where its operating characteristics were measured. The diode was not out of the liquid nitrogen more than a few seconds during transfer to the testing apparatus. After the first set of data was taken, the diode was allowed to warm to room temperature. It was then recooled and the measurements were repeated to determine if any annealing of defects had occurred.

MEASUREMENT OF LASER DIODE CHARACTERISTICS

All laser diode characteristics were measured with the diode immersed in liquid nitrogen except for some preliminary measurements that were taken at room

temperature. Liquid nitrogen was used because of the difficulty of maintaining a constant temperature when the diode was operated in air. Although the temperature of the laser diode was not monitored, heat generated during operation of the device was assumed to be dissipated by the liquid nitrogen.

Power output of the devices was measured with an EG&G 550 multiprobe with the flat filter installed. Because the sensitive area of the detector subtends only a fraction of the laser beam, relative power measurements were taken. To minimize the effects of errors in the alignment of the lasers, a piece of opalized glass was placed against the outside wall of the dewar as depicted in Figure 6. This dispersed the beam so that the position of the detector in the beam was not as critical. Under these conditions, measurements of power output versus input current were reproducible with less than 10 percent deviation in power at a constant current.

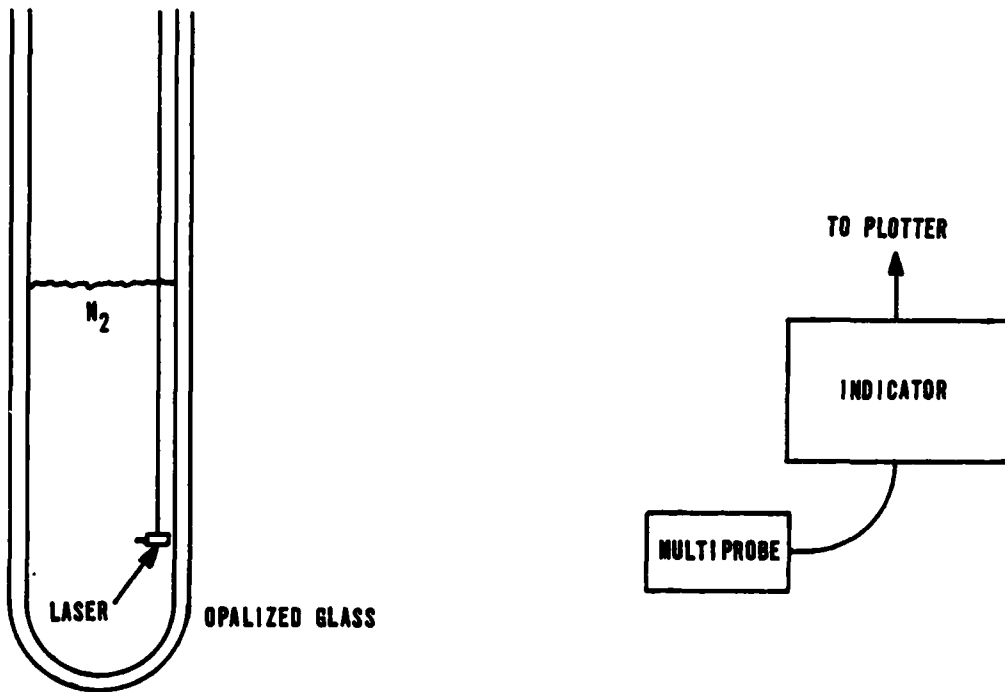


Figure 6. Apparatus for measuring power output.

The output of the multiprobe was connected through an EG&G 450-1 indicator to the y-axis of a Moseley Autograf Model 7001A x-y plotter. The x-axis of the plotter recorded the voltage drop across a 50-ohm resistor in series with the laser diode (Fig. 7). The x-axis was calibrated so that its reading corresponded to the reading of the ammeter in series with the diode.

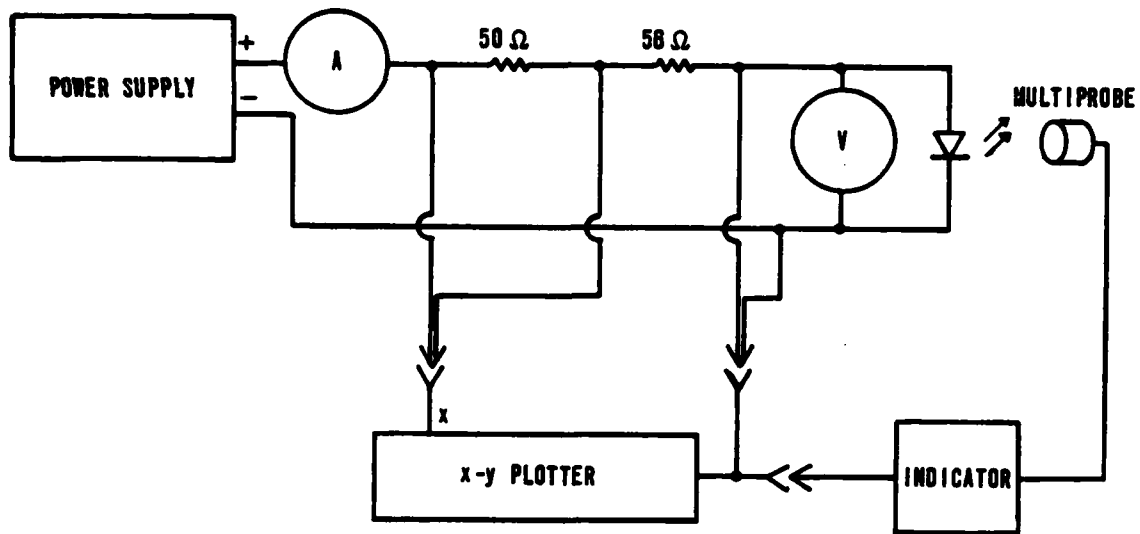


Figure 7. Circuit for measuring power and voltage.

Current versus bias voltage plots were made by disconnecting the radiometer output from the y-axis and connecting the input leads of the laser diode. The current was then increased to the maximum allowed and returned to zero.

The other measurement made for diodes that were irradiated was the spectral output. A Jarrell Ash 0.25-meter Ebert monochrometer with a motor drive was used to measure the spectra of the laser diodes at different operating voltages. The output of a silicon photovoltaic detector and amplifier mounted at the exit slit was connected to the x-axis of the plotter and the y-axis was set to sweep. The sweep was started at a known wavelength and the sweep rate was known, so the wavelength of the peaks could be determined. Additionally, the spectrum of a krypton lamp was superimposed on the laser spectrum when possible.

Voltage and current measurements were made by Honeywell Digitest Model 333 multimeters. The power supply was one side of a Trygon Dual Lab Power Supply, Model DL 40-1. Increases and decreases in bias current were made by manually increasing the power supply voltage.

IV. RESULTS

NEUTRON FLUX MEASUREMENTS

Although the values for the neutron flux published by the Ohio State University Nuclear Reactor Laboratory (NRL) are believed to be correct, nickel flux-monitoring wires were irradiated with each sample. The flux was calculated using the relationship

$$A_0 = N\sigma\phi(1-e^{-\lambda t}) \quad (23)$$

or, for $t \ll t_{1/2}$

$$\phi = A_0/N \sigma \lambda t \quad (24)$$

where ϕ is the flux in $n/cm^2/s$, A_0 is the activity of Co^{58} in the flux wire in disintegrations per second, N is the number of atoms of nickel-58 before irradiation, σ is the cross section for the (n,p) reaction of nickel-58 in the reactor, λ is the decay constant for Co^{58} , and t is the irradiation time.

The flux calculated from the activities of the wires was consistently higher than the value of $3.97 \times 10^{11} n/cm^2-s$ supplied by NRL. The wires were used more than once because of the long half-life of Co^{58} . However, because of the errors that accumulated during successive countings, only the first run for each wire was used. The fluxes calculated from the first runs ranged from $5.97 \times 10^{11} n/cm^2-s$ to $1.03 \times 10^{12} n/cm^2-s$, and averaged $7.78 \times 10^{11} n/cm^2-s$ with an average statistical uncertainty of 3.3 percent. Because of this discrepancy, an aluminum wire was used for one of the irradiations. Results from the (n,α) reaction gave a flux of $9.24 \times 10^{11} n/cm^2-s$, and from the (N,p) reaction gave $7.79 \times 10^{11} n/cm^2-s$. These results confirmed the values obtained with the nickel wires. The best estimate for the flux using calculations from the monitoring wires is $7.94 \times 10^{11} n/cm^2-s$, exactly twice the value supplied by NRL.

Reasons for this discrepancy include either errors in the calculation of the cross sections by NRL, or a perturbation of the neutron flux by the cadmium lining of the sample container. The reactivity effect of the cadmium was -0.24 percent. The effect of this negative reactivity was to decrease the neutron flux, requiring control rods to be pulled farther out of the core to maintain full power. Since the reactor is controlled by monitoring the flux from a point outside the core, the flux at the center of the core may have nearly

doubled, while the flux at the edge of the core decreased sufficiently to keep the total power at 10 kW.

Further experiments are being done to resolve this uncertainty, but, until more is known, values of flux obtained by analyzing the wires will be used. Values reported in this report are based on a flux of 1.68×10^{11} n/cm²-s which is the fast neutron flux (E greater than 0.5 MeV) obtained from the calculations.

IRRADIATION EFFECTS ON LASER DIODES

The performance of the laser diodes was significantly degraded by exposure to the neutron flux. The first diode irradiated, an RCA C30127, No. 70, received a fast neutron fluence of 1.81×10^{15} n/cm². After this irradiation, the diode did not perform as a laser, so the dose for the next diode was reduced by 90 percent.

The other diodes all showed continued degradation with each irradiation. A typical result is shown in Figure 8, the relative power output of RCA diode No. 550 as a function of forward current at several fluences. Two evident effects of irradiation are an increase in threshold current and a decrease in the differential quantum efficiency.

The increase in threshold current for the four diodes that received step irradiations is shown in Figure 9. Threshold current was determined by extrapolating the first increase in the power versus current curve back to the current axis. The point of intersection was taken to be I_{th} . The unirradiated threshold current for the Laser Diode Laboratories' diodes was about twice that of the RCA diodes, and the relative increase in threshold current of the Laser Diode Laboratories' diodes was about twice as high also.

The increases are linear up to a fluence (ψ) of about 10^{15} n/cm², supporting the model developed in Section II. Above this value, the threshold current is higher than that predicted by the linear model. There are several possible causes for this deviation. The most likely is imprecision in measuring the threshold current. There is only one point above 10^{15} n/cm². Although the plots of output versus input current for this fluence show a definite increase in output that extrapolates back to 365 mA, there is a short region of the curve that extrapolates to 310 mA, close to the value predicted by the linear model. Another possibility is that the increase in threshold current is actually greater at higher fluences due to an effect other than the formation of

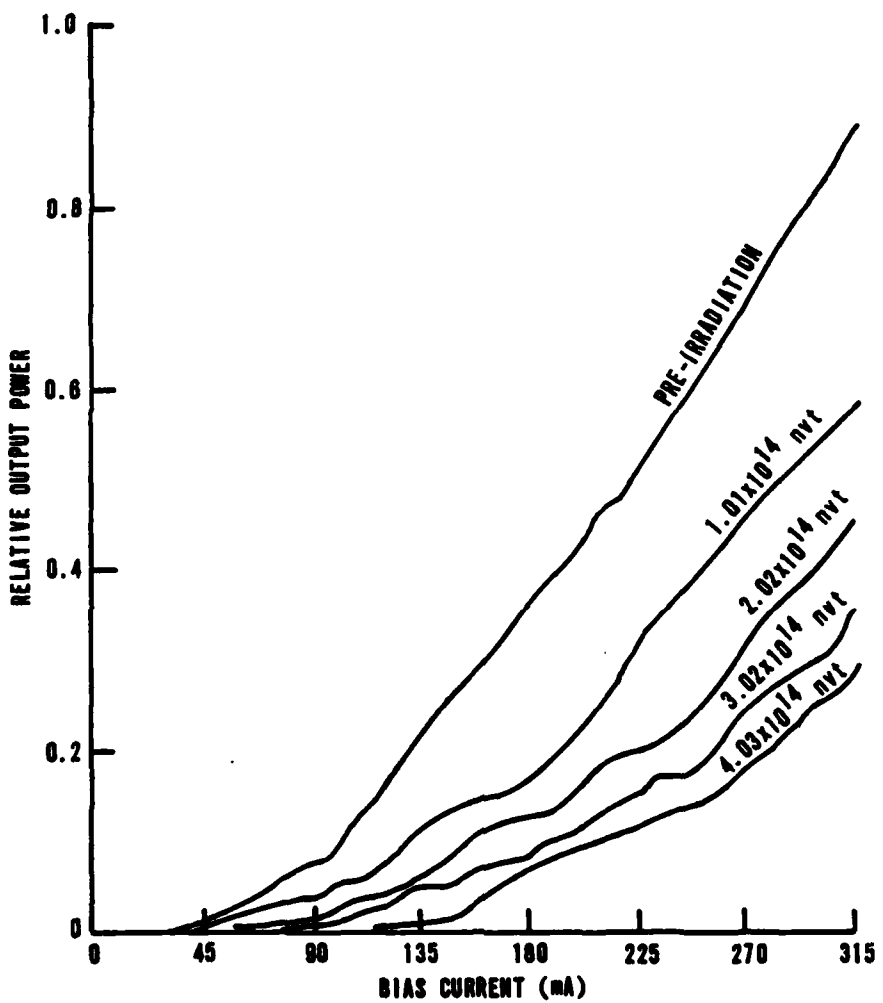


Figure 8. Power vs current of RCA No. 550 at several fluences.

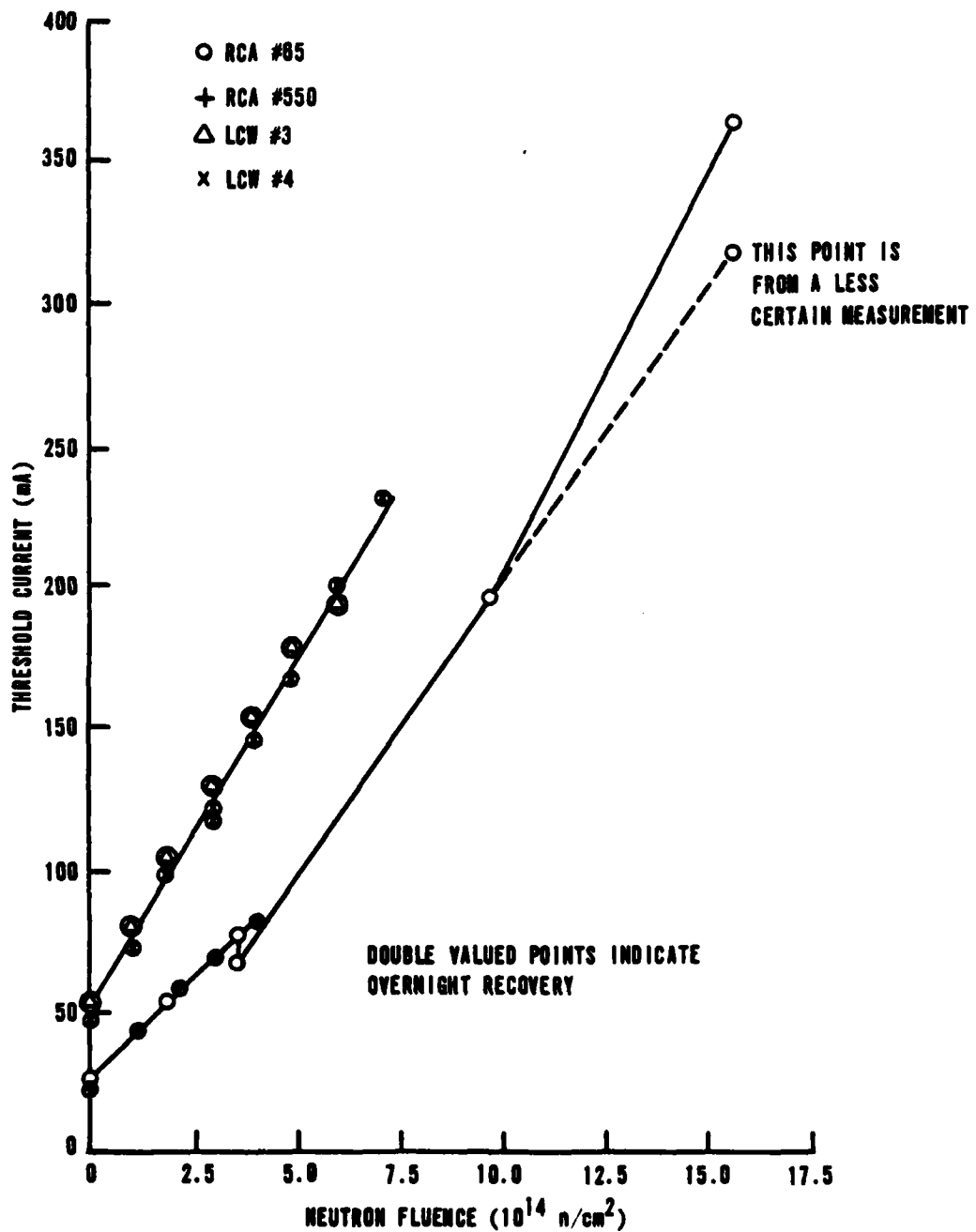


Figure 9. Increase in threshold current vs neutron fluence.

nonradiative centers. This could include an increase in the absorption coefficient in the active region or a loss of some of the wave guiding ability of the heterojunction structure. For the purposes of this report, the reason for the nonlinearity in this region, if it exists, is not important because an increase in threshold current of this amount at 77 K would be an increase to well above the maximum allowed current for the devices at room temperature.

If all four curves for increases in I_{th} with increasing fluence are assumed to be linear, the damage factor, $\tau_0 K_I$, from Equation 20 can be calculated. These factors appear in Table 1. The values of $\tau_0 K_I$ are computed by adding the overnight recovery amount to all measurements taken the next day. The last value for RCA diode No. 65 is not included in the calculation because of its uncertainty. Therefore, the values for $\tau_0 K_I$ in the table should be considered useful only for values of Ψ below about 10^{15} n/cm^2 .

TABLE 1. THRESHOLD CURRENT DAMAGE FACTORS

	$\tau_0 K_I$
RCA No. 65	$5.93 \times 10^{-15} \text{ cm}^2$
RCA No. 550	$5.13 \times 10^{-15} \text{ cm}^2$
LDL No. 3	$4.53 \times 10^{-15} \text{ cm}^2$
LDL No. 4	$5.22 \times 10^{-15} \text{ cm}^2$

The decrease in differential quantum efficiency for each of the four diodes tested in this experimental phase was much more difficult to measure because of the irregular behavior of the output power versus input current curves.

Figure 10 is an example of the large discontinuity encountered in diode No. 65. Although the other diodes behaved less erratically, all exhibited some sort of kink or discontinuity which generally increased in severity as the fluence increased.

The differential quantum efficiency was measured in two ways. First, the slope of the P versus I curve at $(I - I_{th}) = \text{constant}$ was measured graphically by dividing the change in power over a small region by the change in current over the same region. This technique proved to be less than optimum because of the many changes in Δn . The second method was an attempt to find the average Δn over the entire region above threshold. A straight line was drawn using the least squares regression technique that best approximated the P versus $(I - I_{th})$

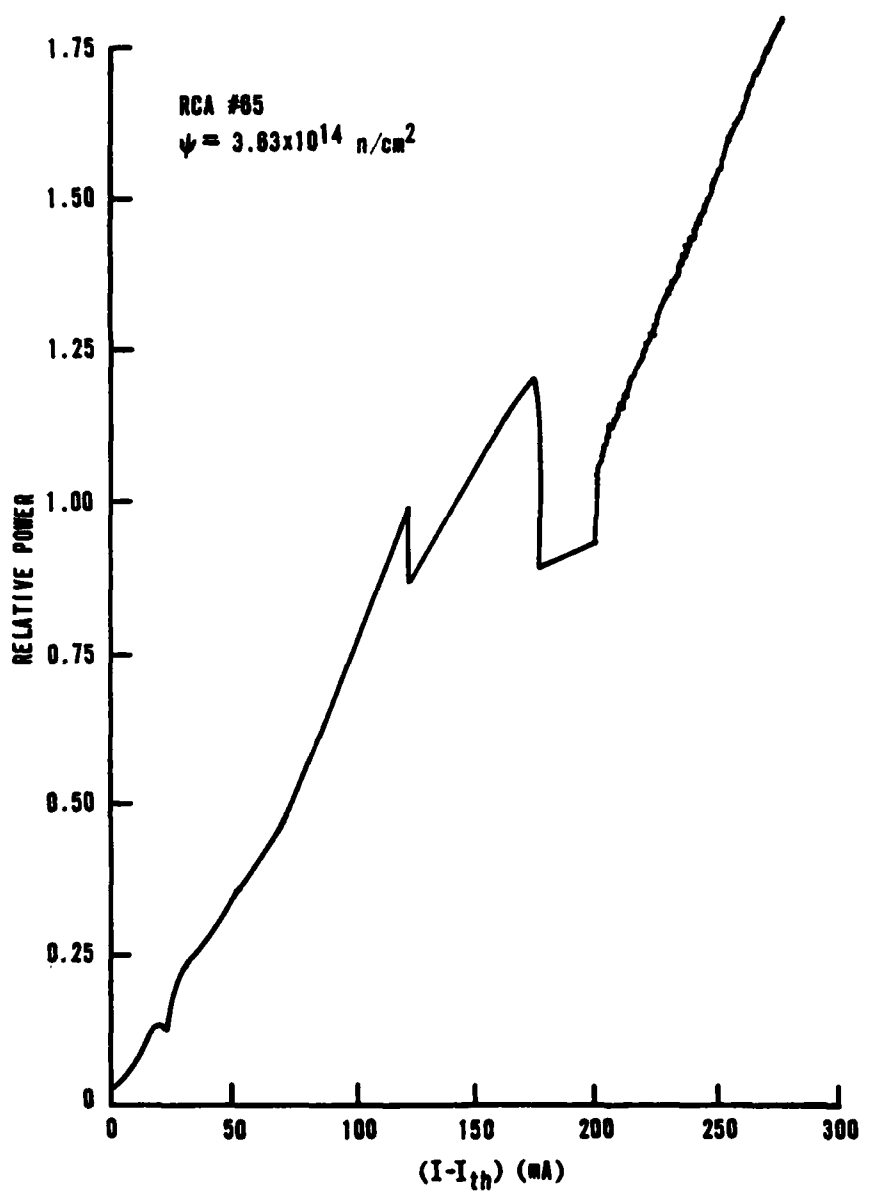


Figure 10. Power vs $(I - I_{th})$ for RCA Diode No. 65.

line, and the slope of this line was taken to be Δn . Since the purpose of this study is to be able to predict the output power of a device at a given neutron fluence, this method was thought to be the most useful. The results of this measurement appear in Figure 11. Although the lines in Figure 11 are not straight as predicted, the varied deviations from linearity do not suggest any

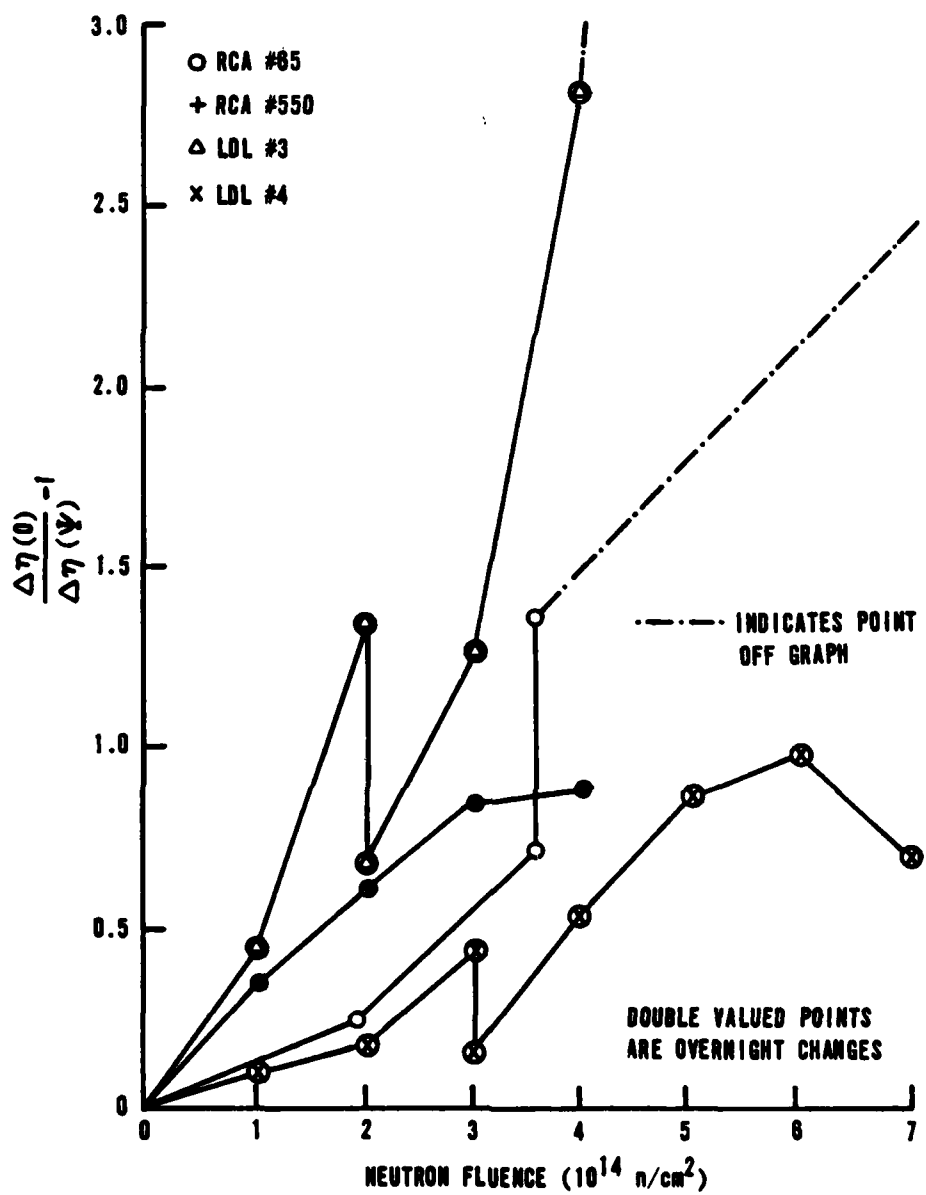


Figure 11. Change in differential quantum efficiency vs neutron fluence.

other trend. The slopes of the straight line approximations to the data in Figure 11 are factors Δn in Equation 21 for each of the diodes. These values are tabulated in Table 2.

The relative output power of each of the four diodes tested is displayed in Figure 12. The sudden drop in power at 3.6×10^{14} for the RCA diode No. 65

TABLE 2. DIFFERENTIAL QUANTUM EFFICIENCY DAMAGE FACTORS

	$\tau_0 K_\Delta$
RCA No. 65	$2.72 \times 10^{-15} \text{ cm}^2$
RCA No. 550	$2.23 \times 10^{-15} \text{ cm}^2$
LDL No. 3	$8.43 \times 10^{-15} \text{ cm}^2$
LDL No. 4	$1.89 \times 10^{-15} \text{ cm}^2$

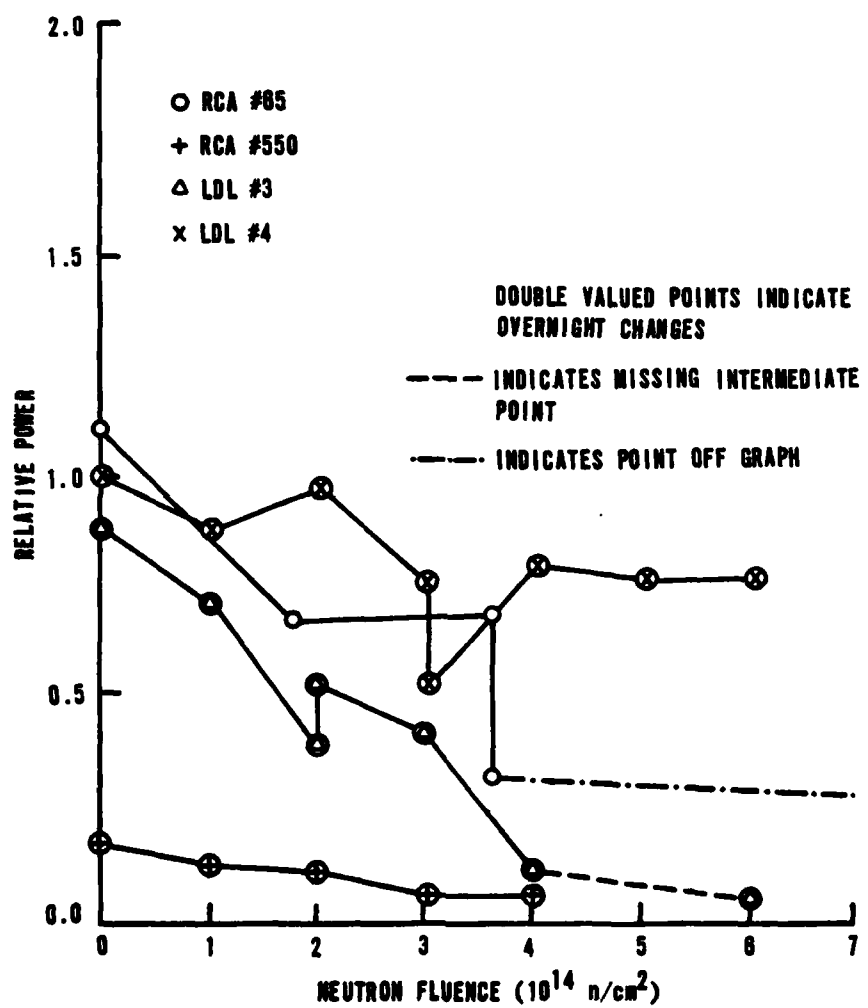


Figure 12. Relative power at 100 mA above threshold vs neutron fluence.

indicates overnight changes in the diode. These values are arbitrary power units taken at 100 mA above threshold for each device. These values are erratic and, for two of the diodes, LDL No. 4 and RCA No. 65, appear to follow no pattern. The other two diodes, LDL No. 3 and RCA No. 550, show an approximately linear decrease in power with increasing neutron fluence. The erratic behavior of the first two curves mentioned is probably due to anomalies in the P versus I curve at $I - I_{th} = 100$ mA. Since two of the diodes show a linear decrease, a linear function for all four may be assumed. The values of $\tau_0 K_p$ from Equation 22 were found by least squares linear regression to $P(0)/P(\phi) - 1$ points with a correction for overnight recovery as described for differential quantum efficiency. The values for $\tau_0 K_p$ are presented in Table 3.

TABLE 3. POWER DAMAGE FACTORS

	$\tau_0 K_p$
RCA No. 65	5.19×10^{-16} cm ²
RCA No. 550	4.05×10^{-15} cm ²
LDL No. 3	9.00×10^{-15} cm ²
LDL No. 4	-7.79×10^{-17} cm ²

The results discussed to this point are useful primarily for verifying the model derived in Section II. For practical purposes, the effect of the neutron fluence on the relative output at a constant current or constant voltage is important. From the damage model, the relative output at constant current as a function of ϕ should be

$$P(\phi) = \Delta n(\phi) (I - I_{th})(\phi) \quad (25)$$

Because of the anomalies in the power output curves, this equation will not predict the power output exactly. The measured relative power at 200 mA for each diode is plotted in Figure 13. As seen, the output power at constant current decreases as the inverse square of the neutron fluence. No single factor was derived for predicting the power output at a constant current because it can be predicted using damage factors already derived, along with Equation 25.

In addition to measurements of power versus current, voltage versus current measurements were taken. A typical plot of V versus I is shown in Figure 14. In this experiment, there was no appreciable change in the voltage required to produce a given current, indicating either that the effect of a neutron fluence

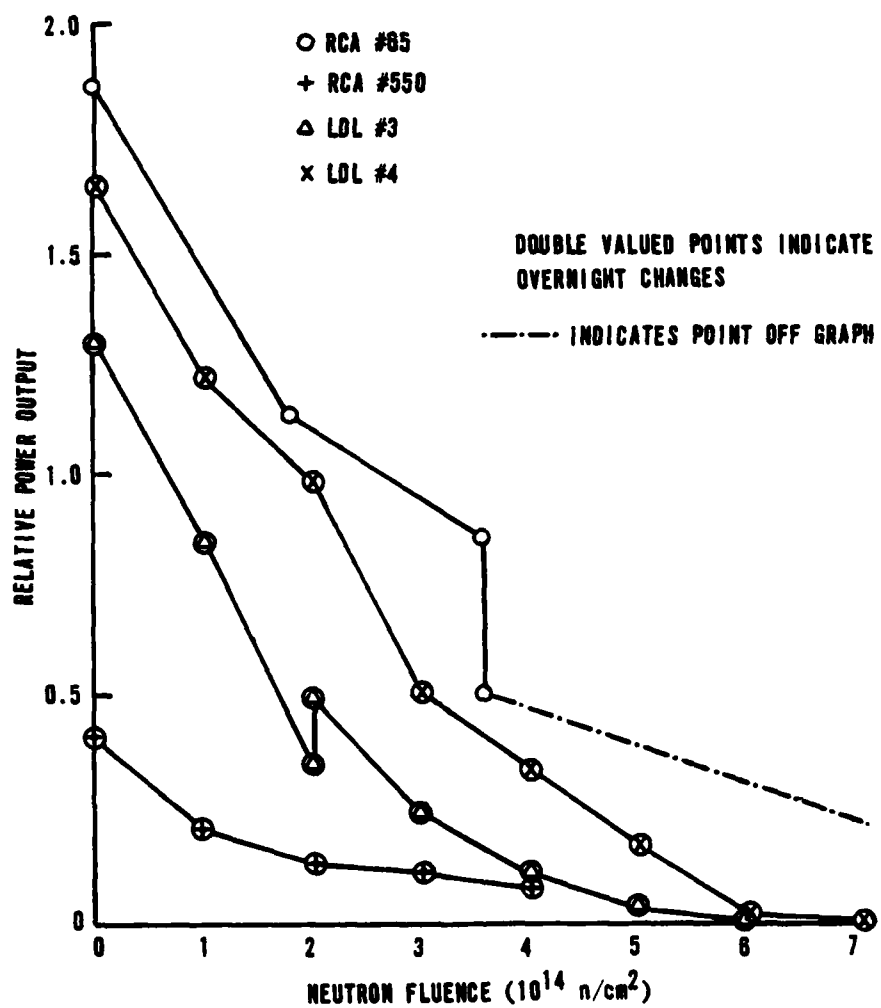


Figure 13. Relative power output at 200 mA vs neutron fluence.

on the diode resistance was very small, or that more than one effect was taking place and the effects nearly canceled each other.

From previous studies, at least two effects on V versus I curves would be expected when a GaAs semiconductor is irradiated with neutrons. Aukerman (Ref. 4) reported an increase in resistivity of the GaAs material with neutron irradiation. Southward (Ref. 6) reported an increase in current at constant voltage for irradiated GaAs diffused laser diodes. The increased current from a decreased carrier lifetime, coupled with increased IR losses, could account for the lack of significant changes in this study. If the change in I versus V was very small, it would not be detectable with the equipment used due to the slope

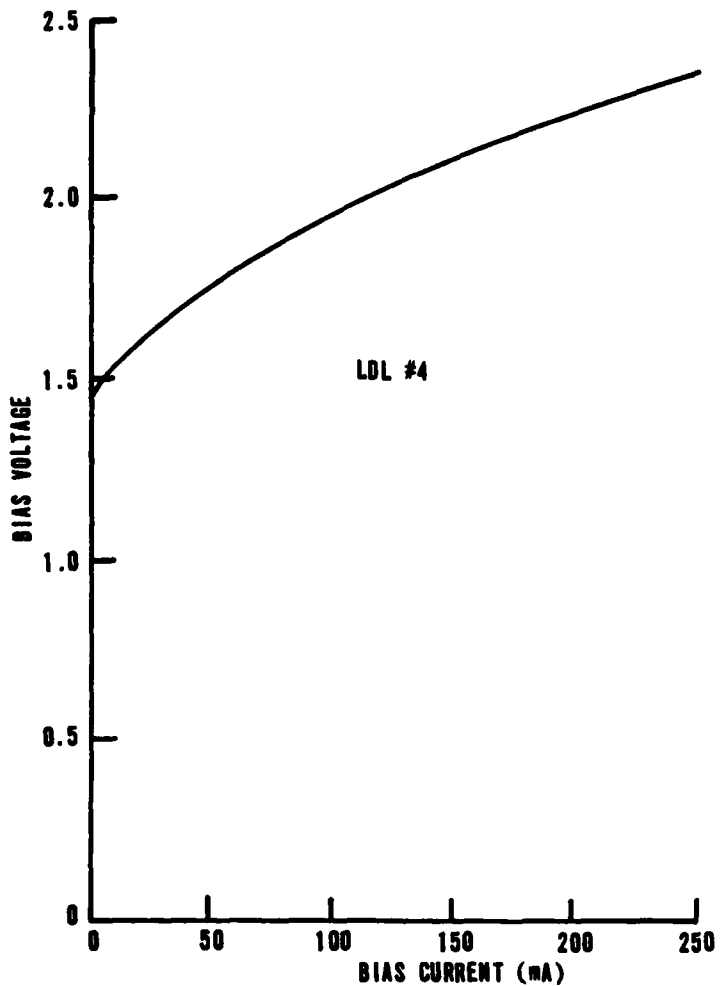


Figure 14. Bias voltage vs forward current.

of the I versus V line in the operating region. For this report, it was assumed that no change in the voltage required for a given current occurred.

The last data taken were spectral measurements of the laser output. After irradiation, there was no significant change in the peak wavelength for lasing, indicating that the neutron fluence did not affect the energy band gap for the lasing transition. There was, however, a shift in peak wavelength with increasing voltage, indicating that the tunneling mechanism described in Section II took place. Additionally, some diodes showed a tendency to lase at two wavelengths separated by about 3 to 4 nm. This suggests that there are two cavities for lasing instead of the one cavity for which the lasers are designed.

The different wavelengths become dominant at different bias currents, but no consistent relationship could be derived.

The results of irradiations at liquid nitrogen temperatures were inconclusive. Because the container could only hold enough liquid nitrogen for a five-minute irradiation, the reduction in power was only slightly more than the reproducibility limits of the measurements (about 10 percent). One diode showed no change in operating characteristics after being warmed to room temperature. The other showed a slight, but insignificant, increase in power output versus current.

V. DISCUSSION AND RECOMMENDATIONS

DISCUSSION OF RESULTS

The results of this work show that AlGaAs, double heterojunction, stripe geometry laser diodes behave much like diffused GaAs lasers when exposed to a flux of fast neutrons. The linear nature of the degradation of threshold current, differential quantum efficiency, and output power at a constant current above threshold suggests that the simple model developed in Section II is probably adequate.

It must be remembered that the damage factors for laser operation were derived from measurements taken at 77 K and not at room temperature. The purpose of immersing the diodes in liquid nitrogen was to provide more control over the operating temperature of the diode. When applying these data to devices operating at room temperature, the fact that preirradiation threshold current is much higher must be taken into account. Moreover, the factor $\tau_0 K_I$ would be expected to be higher because τ_0 is larger at room temperature than at 77 K. The temperature dependence of $\tau_0 K_I$ is demonstrated in the results of Southward's study (Ref. 6). An estimate of the threshold current versus neutron fluence at room temperature is given in Figure 15. Additional study of the operation of these diodes at room temperature must be done before their suitability for use in Air Force systems can be determined.

An interesting and unexpected result of the measurements of power versus current was the significant departure from linearity. Kinks in power output versus current curves have been observed before (Refs. 17, 18, and 19) and explained in a number of ways. Kobayashi (Ref. 18) suggests that the horizontal modes of the laser are unstable and that the number and intensity of these modes changes with the pumping level. As the pumping level is increased, the confinement of the horizontal mode is decreased because the threshold gain region extends farther laterally. This causes the horizontal component of the beam to extend farther away from the center of the device where there is more loss. The result is an increase in the total apparent cavity loss, α , and a reduction in the differential quantum efficiency. Thus, a kink or nonlinearity appears in the output versus current curve of the diode.

Risch, et al., (Ref. 19) have used an external cavity to study the nonlinearities in AlGaAs lasers. They concluded that the internal quantum

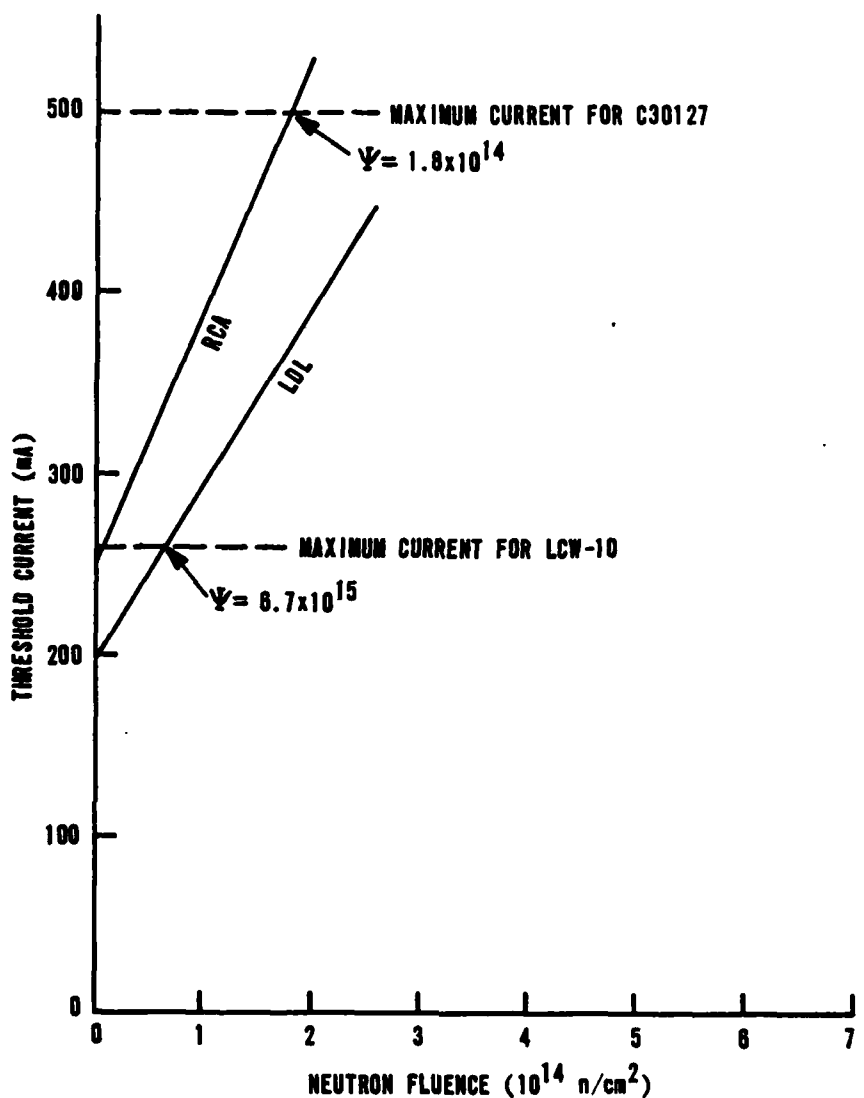


Figure 15. Estimated increase in threshold current vs neutron fluence at room temperature

efficiency of their devices was near 100 percent and was independent of the current density. The anomalies appeared to be related to the ratio between stimulated and spontaneous emission rates (Ref. 19).

The most likely hypothesis in light of the results of the current study is proposed by Campos, et al., (Ref. 17). The fact that the near field transmission pattern changes in the kink region of the laser output led Campos and

his colleagues to believe that the anomalies are due to competition between two cavities within the device. They propose that at low currents, the gain losses are high and the area of least loss determines the lasing cavity. The longitudinal axis of the cavity may be angularly displaced several degrees from the perpendicular to the cleaved ends of the diode. As the current density is increased, the gain throughout the active region becomes more uniform and the mirror losses determine the location of the lasing cavity. Since the factor R is different for the two cavities, the differential quantum efficiency will change when the diode changes cavities and a nonlinearity or kink will appear in the P versus I curve.

Some devices used in the present study showed a tendency for the beam to change direction in the far field as the current was increased. Sometimes the beam would change back to the original direction as current was increased more, and continue to jump back and forth as the current was further increased. The P versus I curve of these devices showed several nonlinearities and some discontinuities. No one else has reported discontinuities in the P versus I curves of laser diodes, and the cause for their appearance is not known. Possibly, the abrupt change of laser cavities as the current is changed also causes the internal quantum efficiency (for stimulated emission), and consequently the power output, of the device to change. Another possibility is that the most intense portion of the beam missed the detector when the laser cavity changed, even with a diffuser near the window of the diode.

Whatever the cause of these anomalies, they are undesirable for communications systems. When the laser is modulated by varying the input current, the output should be linear and at least be single valued for a given current. Devices showing discontinuous behavior, such as the RCA diode No. 65 used in this study would be likely to transmit false information because a discontinuity could be interpreted as a pulse. Although the anomalies disappeared after exposure to higher neutron fluences, moderate fluences caused the discontinuities to become more prominent. If the cavity competition model for the anomalies is correct, the reduction of n_i by irradiation may cause the inhomogeneity to be enhanced, thus intensifying the nonlinear effects.

Another factor which must be considered when using the damage constants obtained in this study is the source of neutrons. According to Lambert, et al. (Ref. 20), the type and dose rate of radiation is important as well as the

total dose. Although the energy spectrum of the neutrons used for irradiation in this experiment may be similar to the air moderated spectrum from a nuclear weapon, there are differences that will give some effect. As the energy of the neutrons increases, an increase in the damage factor would be anticipated.

The dose rate for this experiment was considerably less than that expected from a nuclear blast. Lambert found that neutrons from a high flux accelerator inflicted five times as much damage in semiconductors as the same total dose from a nuclear reactor.

RECOMMENDATIONS

Before using the AlGaAs diode lasers in USAF weapons systems, more studies should be done on radiation effects. The effects of a neutron fluence on room temperature operation should be studied using a high dose rate source. This would give a better estimate of actual performance after a nuclear blast. In addition to the studies of power output, studies of rise time and time delays should be completed.

The data in this experiment were all taken after irradiation was complete, and flux induced charge carriers had recombined. An experiment to determine the transient effects of radiation on the lasers must be done because flux induced currents may damage the devices or associated circuitry significantly.

VI. GAMMA RADIATION-INDUCED EFFECTS

GENERAL

The exposure of AlGaAs lasers to gamma radiation from cobalt-60 (~ 1.25 MeV) introduces defects in the material, in the form of vacancies and interstitials, which affect the performance of the lasers. These defects usually act as non-radiative recombination centers and, since they compete with the radiative centers for the injected carriers, they directly influence such performance parameters as power output, efficiency, and threshold current. Furthermore, if the defects are distributed inhomogeneously in the device, especially in the active region, some effect may be apparent in the output beam characteristics. An inhomogeneous distribution could result from the irradiation method or from device fabrication. Each area will be examined separately.

EFFECT OF GAMMA RADIATION ON CURRENT

Irradiation of AlGaAs lasers with gamma radiation introduces nonradiative recombination centers (Ref. 9). These nonradiative centers have the effect of decreasing the carrier lifetime, τ . Since τ is a factor in both current components, a change in τ will result in a change in the current component. The total lifetime may be expressed as $1/\tau = 1/\tau_R + 1/\tau_{NR}$, where τ_R and τ_{NR} are, respectively, the radiative and nonradiative lifetimes. The introduction of nonradiative centers affects τ_{NR} as illustrated by Equation 26.

$$1/\tau_{NR} = 1/\tau_{0NR} + \sigma_{NRI} V_{th} N_{NRI} \quad (26)$$

where τ_{0NR} is the preirradiation nonradiative lifetime, σ_{NRI} is the capture cross section of the minority carriers, V_{th} is the thermal velocity, and N_{NRI} are the radiation induced nonradiative recombination centers. N_{NRI} can be replaced by $C_I\phi$, where C_I is the rate at which recombination centers are introduced with radiation, ϕ . Equation 26 then becomes

$$1/\tau_{NR} = 1/\tau_{0NR} + \sigma_{NRI} V_{th} C_I \phi \quad (27)$$

The use of Equation 27 allows the total carrier lifetime to be written as

$$1/\tau = 1/\tau_0 + \sigma_{NRI} V_{th} C_I \phi \quad (28)$$

where the subscript 0 denotes the preirradiation value.

The product $\sigma_{NRI} V_{th} C_I$ is usually denoted by K , the damage constant. The effect of radiation on the total lifetime may therefore be written as

$$1/\tau = 1/\tau_0 + K\phi \quad (29)$$

Substitution of Equation 29 in the current equations results in expressions for I_D and I_{SCR} , which contain the effect of radiation. Equation 14 becomes

$$I_D = q A D^{1/2} n_{p0} (1/\tau_0 + K\phi)^{1/2} \exp qV/kT$$

Upon simplification, this expression reduces to

$$I_D = I_{0D} (1 + \tau_0 K\phi)^{1/2} \quad (30)$$

where I_{0D} is the preirradiation diffusion current. Similarly, in the case of I_{SCR} ,

$$I_{SCR} = q n_i w A / 2 (1/\tau_0 + K\phi) \exp qV/2kT$$

This simplifies to

$$I_{SCR} = I_{0SCR} (1 + \tau_0 K\phi) \quad (31)$$

As an example of the effect of radiation on the threshold current, I_{th} , consider a case where the total current flows predominantly by SCR, but light output is due to a diffusion component. Examination of Equations 30 and 31 shows that the effect of radiation would be a reduction in the diffusion, or radiative current component. Since the radiative component determines the threshold, total current would have to be increased until the diminished radiative component is increased to the point where lasing occurs.

EFFECTS OF GAMMA RADIATION ON POWER OUTPUT

Irradiation tends to decrease the optical output of an injection laser by introducing nonradiative recombination centers. The magnitude of the effect of radiation depends strongly on the radiative current flow mechanism in the device. The current flow mechanism, in turn, depends on the operating temperature, the applied voltage, and properties related to device construction.

If the radiative current flow mechanism can be identified, the radiation-induced change in output can be determined. A problem arises when a definite identification cannot be made. This can occur when, at constant temperature and over a specific range of applied voltage, the radiative current flows by a

combination of the mechanisms mentioned earlier. Methods available to identify the radiative current flow mechanism are discussed in the next subsection.

Another factor influencing the measured change in output is the method used to perform the measurement. That is, results will differ depending on whether the measurement is performed at constant voltage or at constant current. A simple explanation for this effect is that at constant voltage additional carriers can be provided, while at constant current this is not possible.

The output of an injection laser may be expressed as

$$P = C \int_0^{\infty} n_p N_A dx \quad (32)$$

where C is a constant, n_p is the electron concentration on the p side, N_A is the acceptor concentration, and the integration is into the p region (Ref. 21). If N_A is assumed to be of the form $a \cdot x^n$, where a is a constant and n is dependent on doping profile, $n = 0$ for an abrupt junction and $n = 1$ for a linearly graded junction, and $n_p = n_{p0} \exp(-X/Le)$ for the case of $\exp qV/kT \gg 1$ (Ref. 11), then Equation 1 can be written as

$$P = C n_{p0} a \exp qV/kT \int_0^{\infty} x^n \exp(-X/Le) dx$$

where Le is the electron diffusion length. Upon evaluation of the integral and substitution of $Le = (D\tau)^{1/2}$, this expression becomes

$$P = C n_{p0} a \exp qV/kT n! (D\tau)^{\frac{n+1}{2}} \quad (33)$$

Substitution of Equation 29 in Equation 33 yields, after simplification

$$\left(\frac{P_0}{P}\right)^{\frac{2}{n+1}} = 1 + \tau_0 K \phi \quad (34)$$

where P_0 represents the preirradiation output. Equation 34 expresses radiation-induced change in a diffusion controlled output when measured at constant voltage.

If the measurement is performed at constant current, Equation 14 must be solved for V and the result substituted into Equation 33. Substitution yields, after simplification,

$$P = C_1 \tau^{\frac{n+2}{2}} I_D$$

where the constants have been collected in C_1 . Use of Equation 29 on this expression yields

$$(P_0/P)^{\frac{2}{n+2}} = 1 + \tau_0 K\phi \quad (35)$$

The total current in these devices, especially at low temperature and low supplied voltage, usually flows by SCR. Thus, to determine the change in output due to damage in the space charge region, the equation for total current is used, or $I_{tot} \approx I_{SCR}$. For a constant current measurement, Equation 15 is solved for V and the result is substituted into Equation 33. The result is

$$P = C_2 \tau^{\frac{n+5}{2}} I_{SCR}^2$$

The use of Equation 29 results in

$$(P_0/P)^{\frac{2}{n+5}} = 1 + \tau_0 K\phi \quad (36)$$

If the output is due to radiative recombination in the space charge region, then for a constant voltage measurement, the effect of gamma radiation is negligible. This is the case since the recombination rate through a particular type of center in the space charge region is controlled by the quasi-Fermi levels. These levels are affected by applied voltage and doping, but not by irradiation unless the amount of radiation is sufficient to cause a significant removal of carriers in the neutral regions.

DETERMINATION OF CURRENT FLOW MECHANISMS

It has been indicated that radiation-induced changes in output are dependent on the current flow mechanism responsible for the radiative transitions. The mechanisms of concern are diffusion and SCR.

A tentative identification of the current mechanisms can be made by examination of the P-V and I-V curves. Diffusion current may be written as $I_D = C_1 \exp qV/kT$ and SCR current as $I_{SCR} = C_2 \exp qV/2kT$, where C_1 and C_2 are constants containing all the factors as given in Equations 14 and 15. Thus, if current

is plotted versus voltage on a semilog graph, a slope of q/kT indicates a diffusion process and a slope of $q/2kT$ indicates an SCR mechanism. When current is plotted versus voltage, the values of current represent the total current. Similarly, when output is plotted versus voltage, the slope of the curve gives an indication of the current flow mechanism responsible for the radiative transitions.

A further means of identification is due to the differing effects of radiation on diffusion controlled and SCR controlled output. The effect of radiation on diffusion output is much more pronounced than on SCR output. Comparison of the preirradiation P-V curve with the post-irradiation P-V curve may, over a range of V , show a significant difference, indicating diffusion controlled output, or may show only a slight change, indicating SCR controlled output.

SHIFT OF EMISSION PEAK

A shift in energy of the emission peak may occur with a change in the applied voltage. If this happens, it is an indication of the presence of a radiative current due to a tunneling mechanism. Tunneling probability is highest near the respective quasi-Fermi levels of the carriers (Ref. 22). The level separation is directly dependent on V . Thus, a change in applied voltage causes a change in level separation and a photon emitted as a result of a tunneling process reflects this energy shift. The tunneling current may be expressed as

$$I_{\text{tun}} = B \exp (\alpha_t V) \quad (37)$$

where B is a constant containing dopant concentration and α_t depends on the shape of the junction and also contains dopant concentration. The only radiation-sensitive quantity in Equation 37 is the dopant concentration. This means that a radiation induced change in the tunneling current only becomes evident when the amount of radiation is sufficient to remove a significant number of carriers by effectively changing the dopant concentration. Share, et al. (Ref. 10), invoked the concept of the luminescent killer center to explain the peak shift with irradiation. Assuming donor-acceptor pair radiative transitions, the shift to higher energies can be explained if the more distant pairs are removed from the radiative process by the killer centers.

RADIATION INDUCED BEAM CHANGES

The shift of the emission peak with irradiation has just been discussed. Changes in the axial mode structure of the emitted light are not anticipated since these modes are not determined by any radiation sensitive quantities. Changes in the transverse modes could occur if radiation affected the properties of the active region. Transverse mode separation is given by

$$\Delta\lambda/\Delta m = -\lambda^2/2\pi n_e x_0 \quad (38)$$

where n_e is the wavelength dependent index of refraction and x_0 represents a constant which measures the rate of decrease of the index of refraction either parallel or perpendicular to the junction, depending on which case is considered (Ref. 11). The effect of radiation on the wavelength is minimal, but the introduction of nonradiative recombination centers may change the wave-guiding properties of the cavity. This effect would be manifested by a change in the product of the effective refractive index and the index rate of change. A change in the wave-guiding characteristics of the cavity would appear as changes in the intensity distribution of the beam and in changes in beam divergence.

VII. DESCRIPTION OF SAMPLES AND EXPERIMENTS

The injection lasers used in this study were type C30127 from RCA and type LCW-10 from Laser Diode Laboratories, Inc. Both types were designed to operate in the continuous wave mode at room temperature. Relevant performance characteristics, as provided by the manufacturers, are given in Table 4. Specific information was provided with each sample and is listed in Table 5. Detailed information about these AlGaAs lasers was considered proprietary by the manufacturers and could not be obtained.

TABLE 4. TYPICAL OPERATING CHARACTERISTICS AT ROOM TEMPERATURE AS PROVIDED BY MANUFACTURER

Parameter	LCW-10	C30127	Units
P_o (max)	14	15	mW
I_{th}	200	250	mA
Emission Peak	850	820	nm
Beam Spread			
Parallel	5	5	deg, HWHM
Perpendicular	20	20	deg, HWHM

TABLE 5. SPECIFIC INFORMATION PROVIDED BY MANUFACTURER

Type	Sample	I_{th} (mA)	I_{max} (mA)	P_o (mW)
LCW-10	1	180	230	11.6
LCW-10	2	210	260	12.5
C30127	66	240	500*	5 at 260 mA
C30127	68	210	500*	5 at 245 mA

* I_{max} provided as 500 mA for all type C30127 samples.

Initial measurements were performed at room temperature prior to irradiation to verify the manufacturer's data. Then the initial experiments were repeated at liquid nitrogen temperature since post-irradiation measurements were to be conducted at that temperature.

Preirradiation experiments determined the I-V and P-V relationships, the intensity distribution in the beam and the divergence, the spectral distribution

at various, arbitrarily selected forward currents, and the emission peak shift as a function of applied voltage. Additionally, output, power efficiency, differential external quantum efficiency, and threshold current information were obtained.

To obtain the I-V and P-V information at room temperature, the circuit depicted in Figure 16 was used.

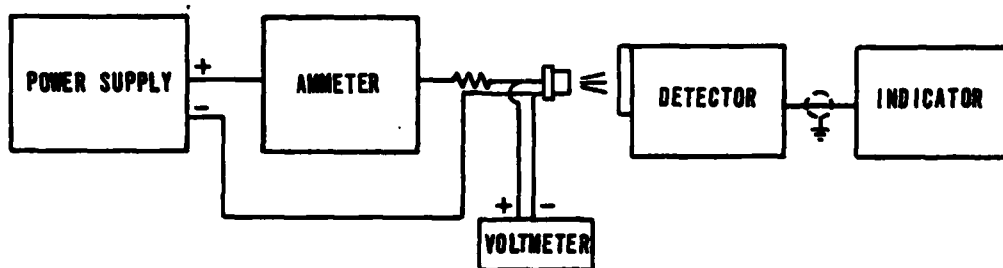


Figure 16. Circuit for measuring I-V, P-V relationships.

The laser device was attached to a heat sink capable of dissipating 2 watts and a resistor, R, was placed in the circuit to eliminate current spikes (14Ω , 10 W). The injection current was provided by a Trygon Electronics Model DL 40-1 power supply and was measured with a Honeywell Digitest Model 333. The voltage across the device was also measured with a Model 333. The laser was centered at a distance of 1.5 cm from the input aperture of the EG&G Model 580-11A Detector and the laser output was displayed by the Model 580-11A Indicator Unit.

Data were obtained by adjusting the power supply to a specific current, as presented by the ammeter, noting the corresponding voltmeter reading and the detector current displayed by the indicator unit. After each reading, the power supply output was reduced to zero to avoid heating effects.

The values obtained were readily converted to power supplied ($I_F \times V$), power output of the laser (detector current \times constants supplied with Model 580-11A radiometer), and power efficiency (ratio of the powers). The P-V, I-V, and P-I relations could then be plotted and the threshold currents obtained from the P-I plots.

The combination of heat sink and reduction of the output of the power supply to zero between readings kept the temperature at each individual reading

within 1°C of room temperature. The heat sink alone allowed a rise of 2° to 3°C above room temperature at forward currents ~50 percent above threshold when power was applied continuously for a period of approximately 5 minutes.

Intensity distribution was obtained by mounting the laser on a movable carriage at a fixed distance, in the far field, from the detector head input plane and illuminating a hole 0.5 mm in diameter. The position dependent angle was then calculated and related to the laser output as represented by the detector current. Again, the power supply output was reduced to zero between readings. Laser output was then plotted against the calculated angle and the beam divergence in degrees at the 50 percent points was read from the plot.

To obtain spectral information a configuration as shown in Figure 17 was used.

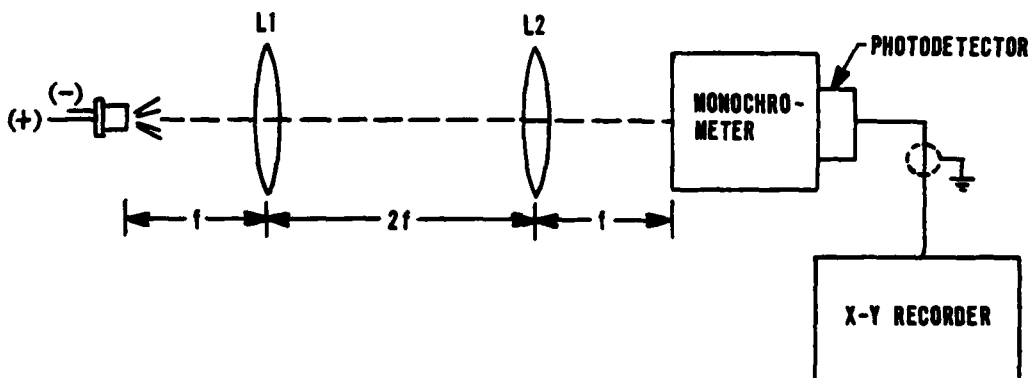


Figure 17. Configuration for obtaining spectral data.

Lenses 1 and 2 were identical (dia = 3 cm, $f = 50.8$ mm) and focused the laser light on the entrance slit of the 0.25 m Ebert monochromator. A Si photodetector (HAV1000) was attached to the exit slit and provided the input for the H-P/Moseley Model 7001 X-Y recorder. Best results, in terms of resolution, were obtained with the smallest available slits, 25 mm. The circuit shown in Figure 16 was used and the laser operated at arbitrarily selected forward currents above threshold. The system was aligned by using an IR detector plate to focus the light on the entrance slit and by monitoring the pen deflection of the recorder. When necessary, neutral density filters were used immediately in front of lens 2 to reduce the input to the photodetector. The spectral plots were obtained by selecting an appropriate starting point for the scan, adjusting recorder sensitivity and scan speed, adjusting the power supply to the

desired forward current, and simultaneously activating monochromator and recorder scan.

As stated, these measurements were then repeated at liquid nitrogen temperature. In this case, the samples were attached to a glass rod and were totally immersed in the liquid. The experimental configuration was the same as described above, except that the laser output had to penetrate the double walls of the dewar. Since this study was concerned with relative effects, this was not considered a problem. As at room temperature, the power supply was returned to zero between readings.

The samples were irradiated by placing them in the exposure chamber of a cobalt-60 source for the length of time required to absorb a predetermined dosage. The orientation of the samples in the chamber was random. Exposure to 10^7 rad(Si) was done at the Air Force Institute of Technology's Nuclear Center, and exposure to 10^8 rad(Si) was conducted at the Gamma Irradiation Facility of the Sandia Laboratories.

Initially, only one sample was irradiated to 10^4 rad(Si) to observe the severity of the effects. After analyzing performance changes the same sample was irradiated to 2×10^4 and 5×10^4 rad(Si), with measurements being taken after each exposure. Only then, after having obtained a general idea of radiation induced degradation, were the other samples irradiated to 10^4 rad(Si). Since samples 66 and 68 exhibited a rapid drop in performance, they were irradiated to 10^5 , 5×10^5 , and 10^6 rad(Si). The intermediate levels were not thought necessary for samples 1 and 2 since they showed no decrease in performance after the first exposure. Irradiation was done at room temperature, subsequent measurements at 77 K.

VIII. RESULTS AND DISCUSSION

GENERAL

The results of the measurements are presented and discussed separately. Factors influencing the accuracy of the measurements are considered in each case, and when possible, the measured effect has been attributed to the responsible physical mechanism.

PREIRRADIATION PERFORMANCE

The measured values of the threshold current, I_{th} ; the output power, P ; and the position of the emission peak are listed in Table 6 for comparison with the data provided by the manufacturers. The temperature of the laser case, T_c , at which the measurements were performed, is also given. I_{th} was determined by extrapolating the linear portion of the $I-P$ curve to the I axis. This method of obtaining the values of I_{th} may partially account for the difference between the manufacturers' and measured values. Another factor to account for the difference could be the temperature of the measurements. Temperature strongly affects I_{th} and it was not known at what room temperature the manufacturers performed their measurements.

Temperature also affects the output power and may be one of the causes of the difference. Errors in the power due to equipment and procedure are limited to ± 6 percent of the values given. The emission peak position was obtained by placing an envelope over the emission spectrum and using the highest point. In view of the limitations of the equipment used for this measurement, the given values of the emission peaks must be considered as representative only, rather than as absolute.

TABLE 6. MEASURED PREIRRADIATION CHARACTERISTICS AT ROOM TEMPERATURE

Type	Sample	I_{th} (mA)	P (mW) at I (mA)	T_c (K)	Emission Peak (nm)
LCW-10	1	165	12.6 at 230	296	883
LCW-10	2	195	11.8 at 260	297	884
C30127	66	235	6.9 at 260	294	819
C30127	68	240	1.6 at 245	296	821

The same measurements, performed at liquid nitrogen temperature, resulted in the values given in Table 7.

TABLE 7. MEASURED PREIRRADIATION CHARACTERISTICS AT 77 K

Type	Sample	I_{th} (mA)	P (mW) at I (mA)	Emission Peak (nm)
LCW-10	1	60	44.2 at 200	829
LCW-10	2	70	51.2 at 200	839
C30127	66	30	81.1 at 200	764
C30127	68	30	31.3 at 200	768

All samples except 66 presented smooth I-P curves. Sample 66 exhibited a kink at room temperature and at 77 K. This kink has been explained as being due to unstable horizontal modes (Ref. 18) and cavity competition (Ref. 17). Additionally, each sample exhibited an apparent shift of emission peak with applied voltage, indicating the presence of a tunneling mechanism (Ref. 22). Shift of emission peak with applied voltage is shown in Figures 18 and 19.

The intensity distribution and divergence were measured in the far field at room temperature only. The preirradiation values of the beam divergence were found to agree closely with those given by the manufacturers. Pre- and postirradiation intensity distributions are presented together later for comparison purposes.

The I-V and P-V curves for four samples are shown in Figures 20a and 20b. The differences in slope between the output and current curves are readily apparent, indicating different mechanisms for the total and radiative current flow. The bending of the output curves at higher values of V should be noted. It could be due to the expected increase in resistive losses, or to a change in the radiative current flow mechanism.

The information used to generate the I-V and P-V curves was also used to plot power efficiency. Power efficiency is defined as the ratio of the output power and the supplied power, or P_{out}/IV . The power efficiencies for the samples are shown in Figures 21a and 21b.

MEASURED EFFECT OF RADIATION ON THRESHOLD CURRENT

As stated earlier, the initial exposure of the samples was to 10^4 rad(Si). Subsequent exposures raised the dosage to 10^8 rad(Si). I_{th} was determined from the I-P curves as before. Figures 22a through 22d present the current-output relationships for the different levels of irradiation, and Table 8 gives the values of the threshold current as a function of dosage within ± 5 percent.

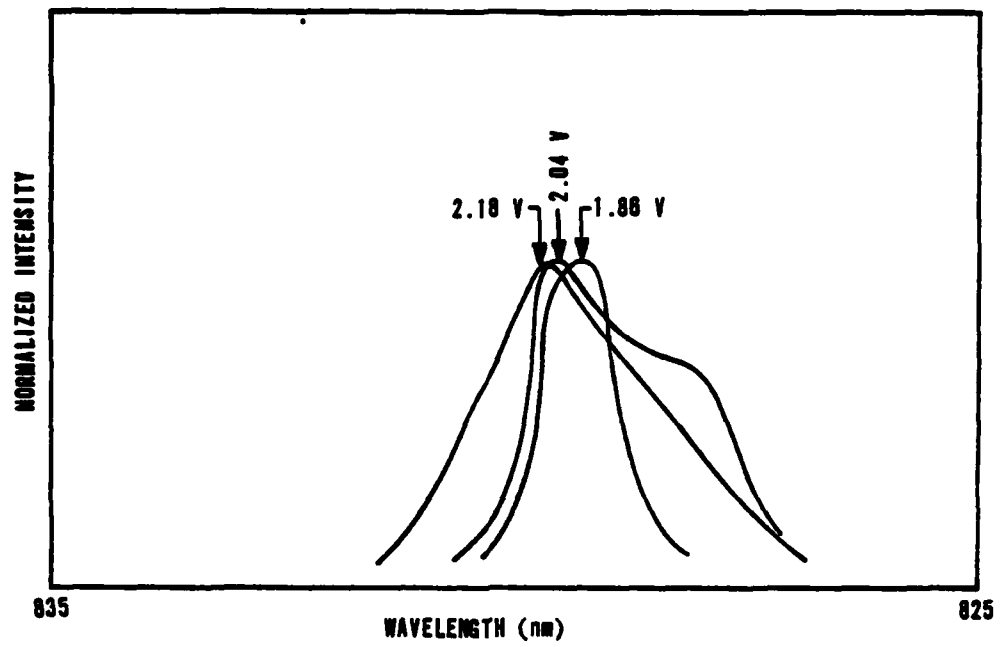


Figure 18a. Shift of emission peak with applied voltage at 77 K, preirradiation, sample 1.

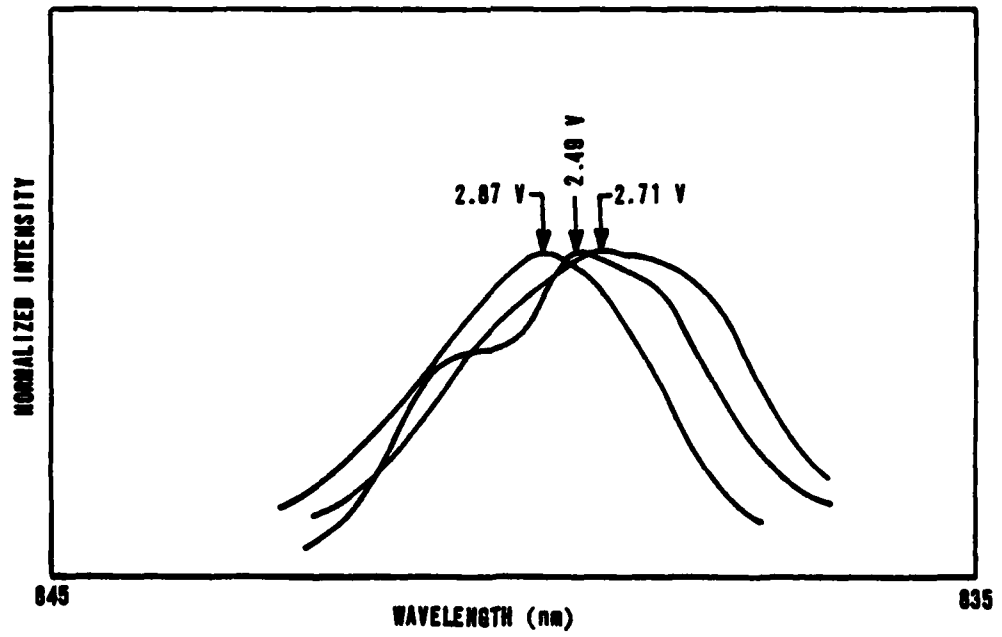


Figure 18b. Shift of emission peak with applied voltage at 77 K, preirradiation, sample 2.

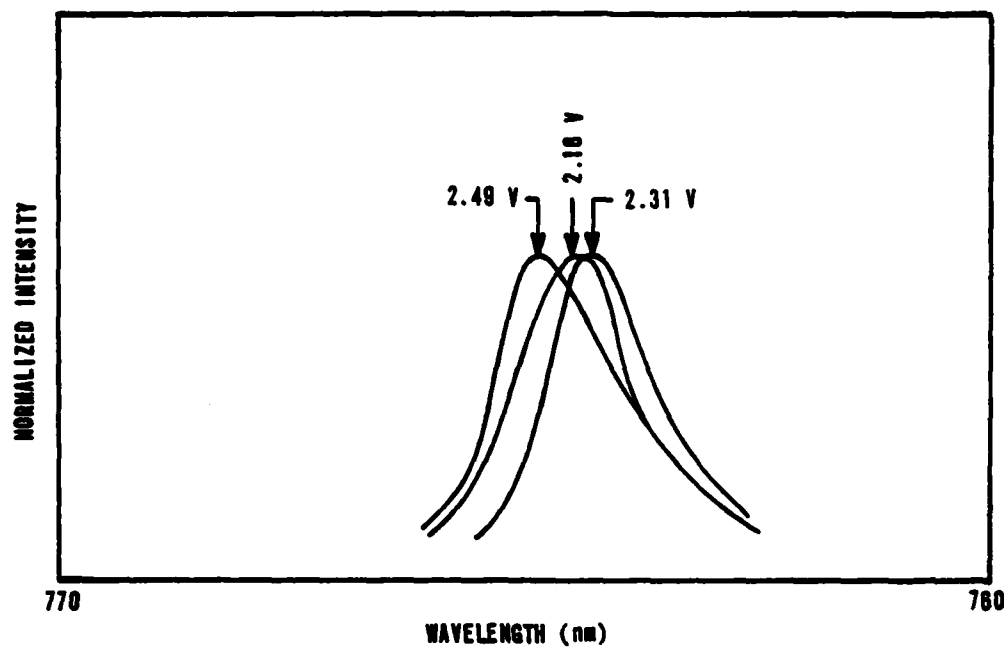


Figure 19a. Shift of emission peak with applied voltage at 77 K, preirradiation, sample 66.

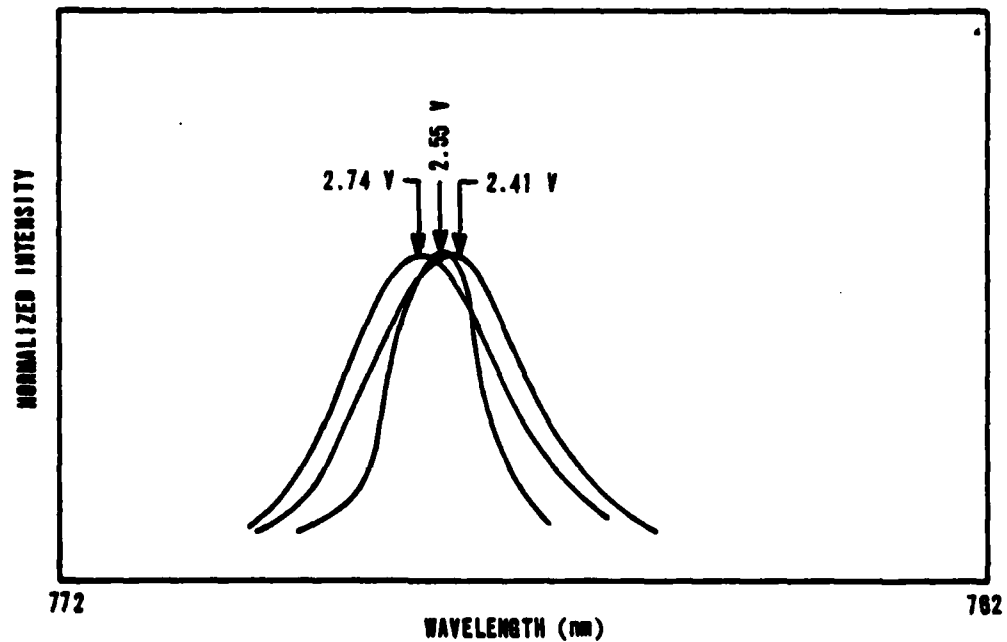


Figure 19b. Shift of emission peak with applied voltage at 77 K, preirradiation, sample 68.

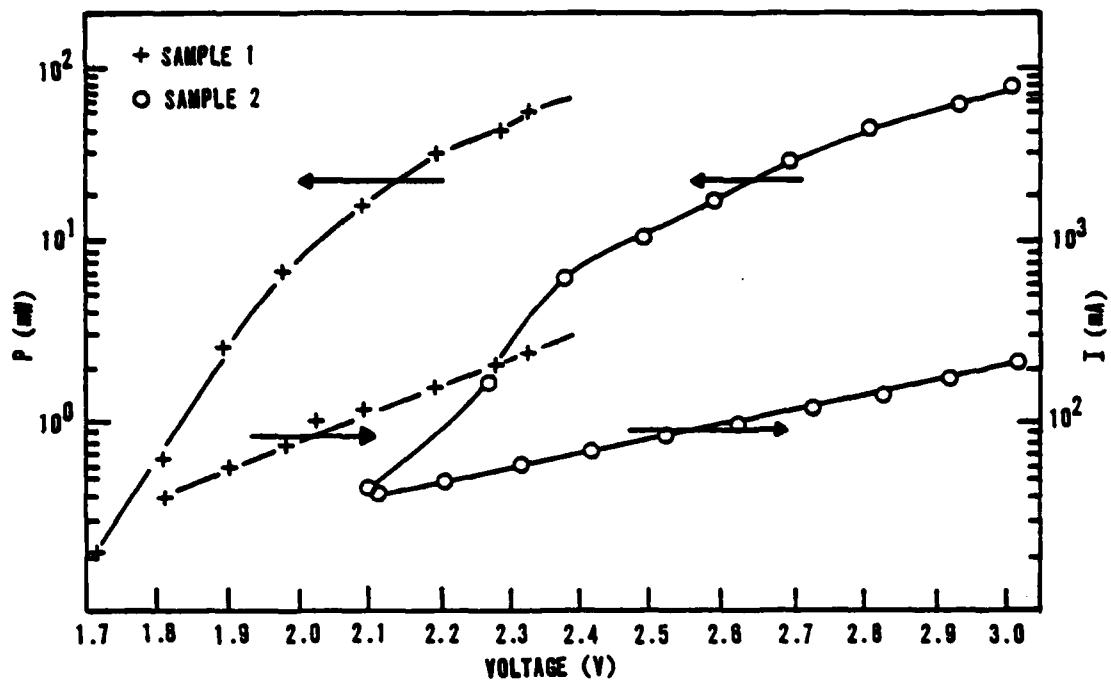


Figure 20a. Preirradiation power-voltage and current-voltage relation at 77 K.

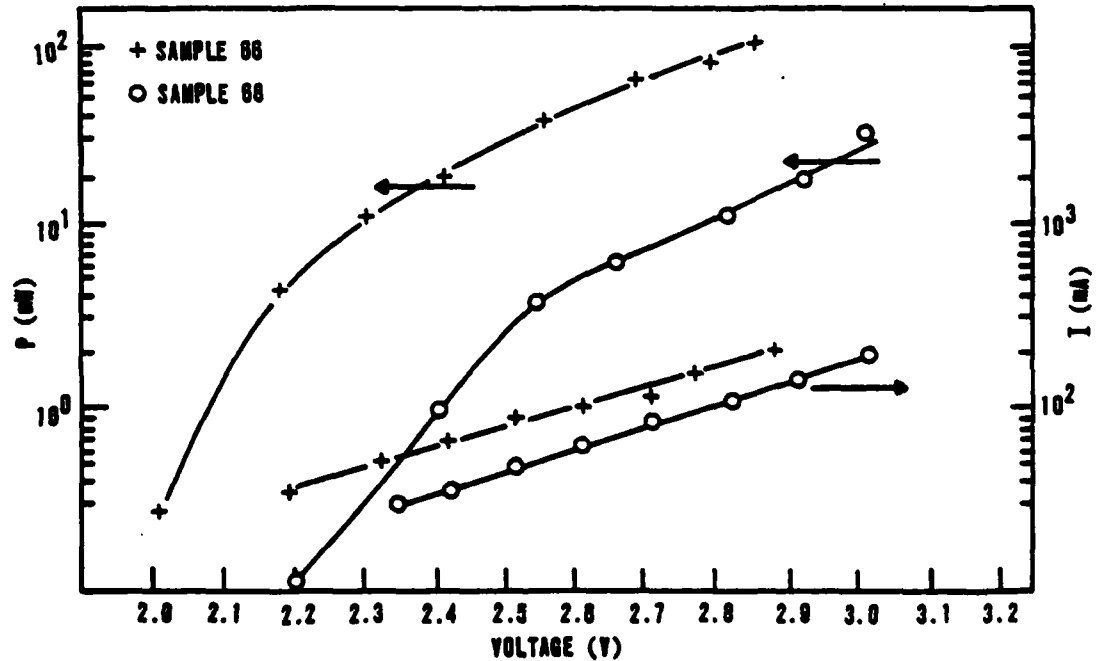


Figure 20b. Preirradiation power-voltage and current-voltage relation at 77 K.

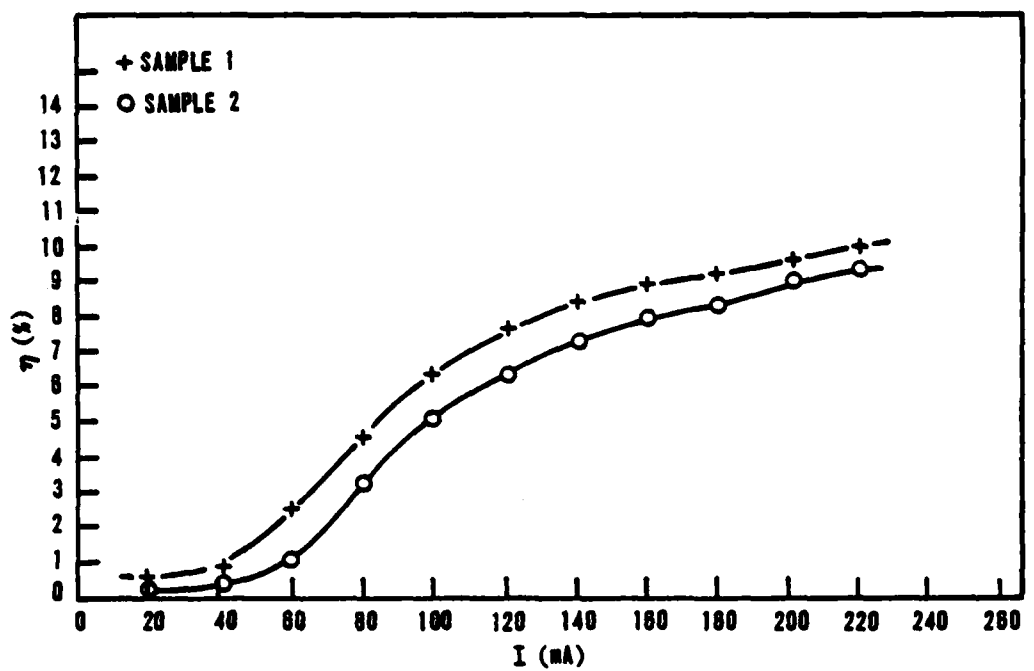


Figure 21a. Preirradiation power efficiency at 77 K.

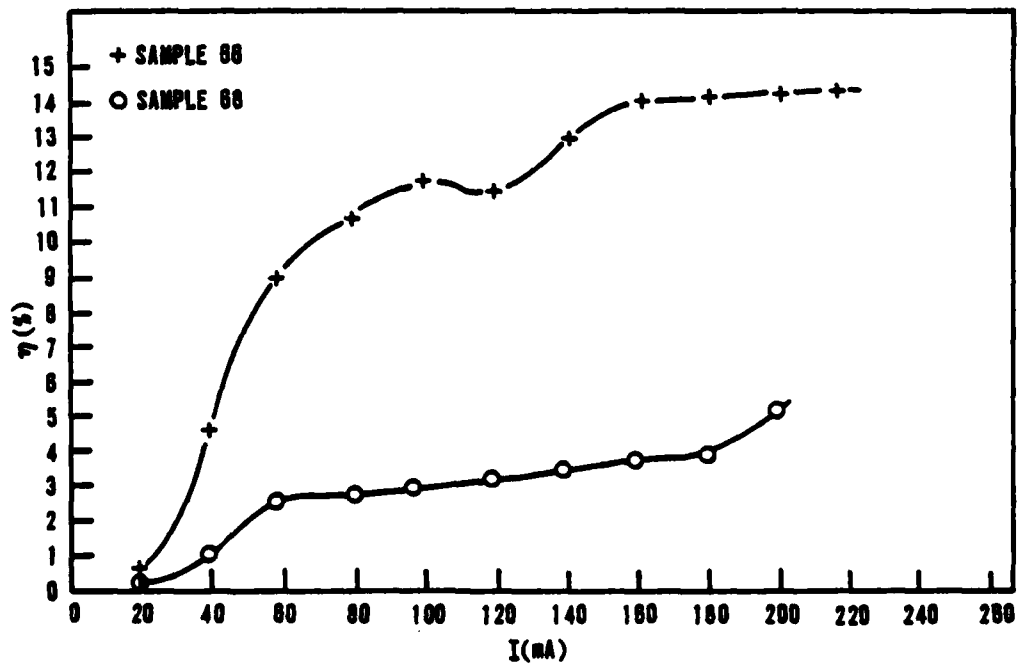


Figure 21b. Preirradiation power efficiency at 77 K.

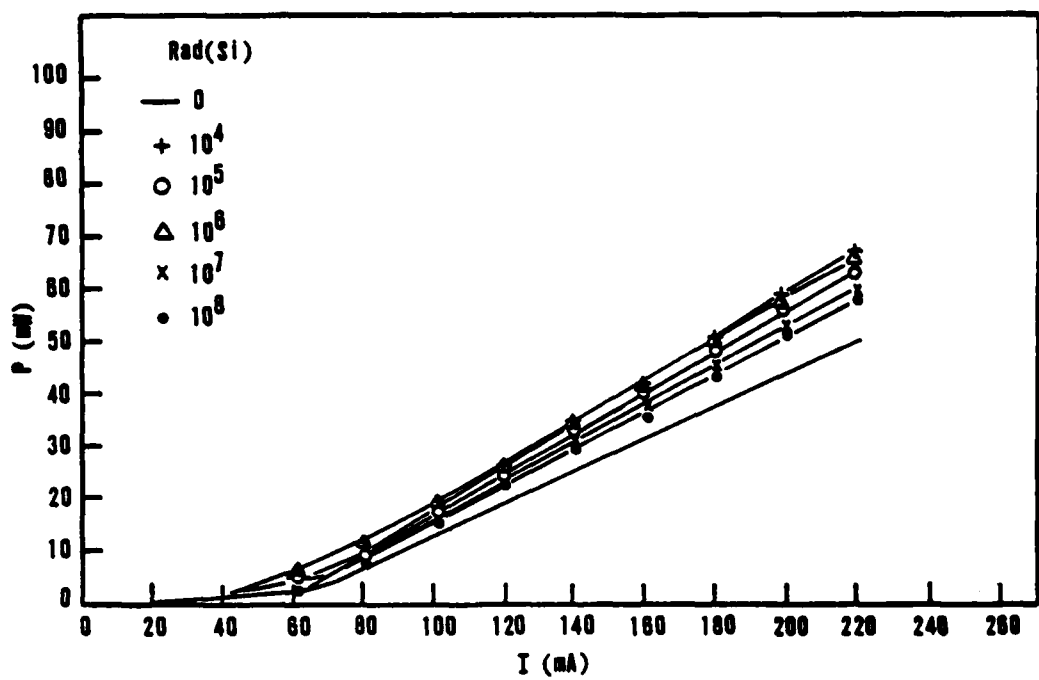


Figure 22a. Power-current relation as function of dosage at 77 K, sample 1.

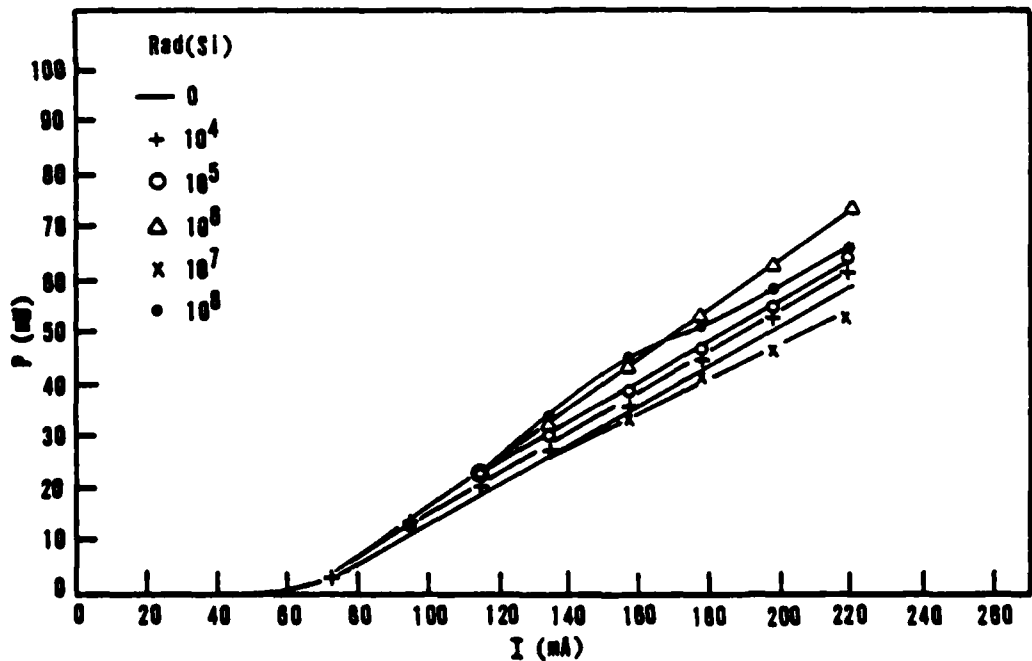


Figure 22b. Power-current relation as function of dosage at 77 K, sample 2.

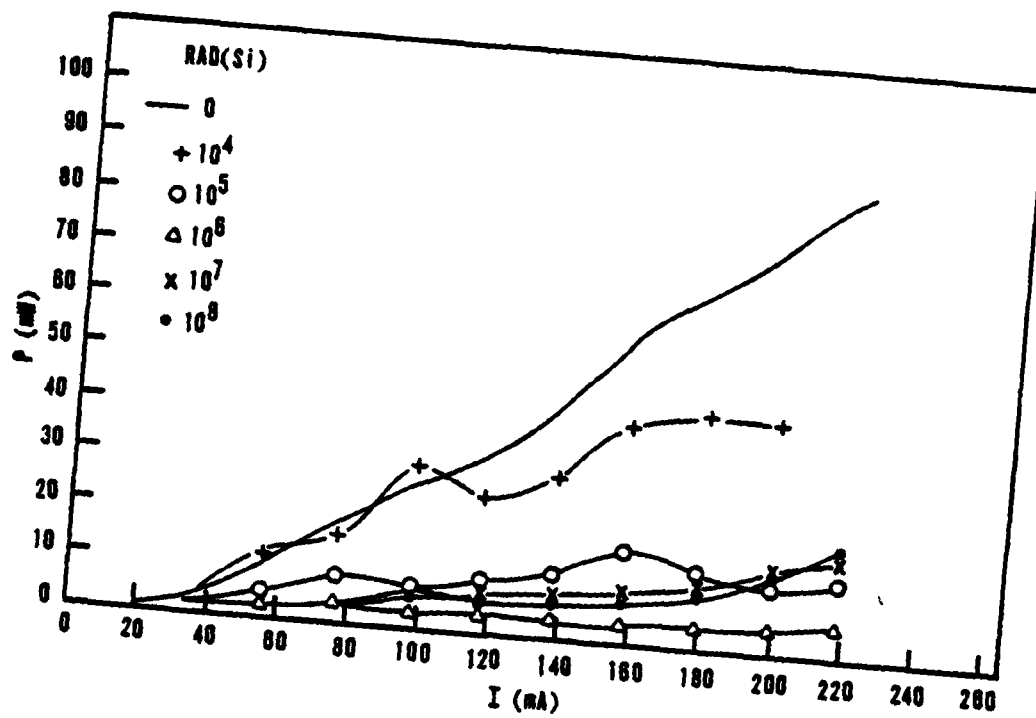


Figure 22c. Power-current relation as function of dosage at 77 K, sample 66.

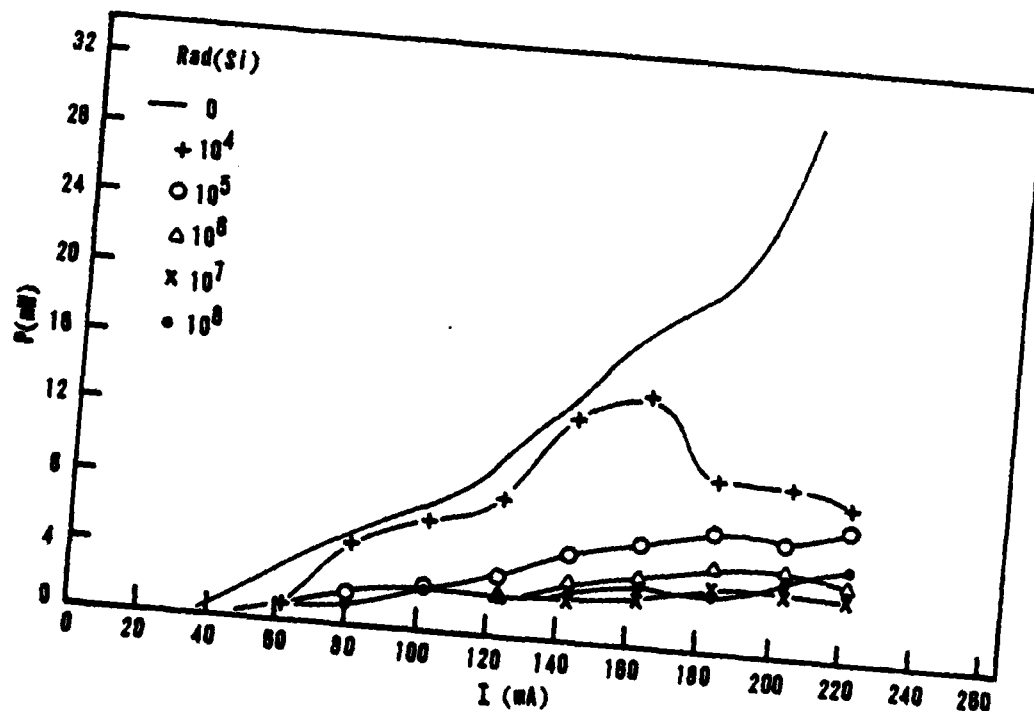


Figure 22d. Power-current relation as function of dosage at 77 K, sample 68.

TABLE 8. THRESHOLD CURRENT AS FUNCTION OF DOSAGE

Sample	I_{th}^1 (mA)	I_{th}^2 (mA)	I_{th}^{66} (mA)	I_{th}^{68} (mA)
0	60	70	30	30
10^4	60	70	35	35
10^5	60	70	35	70
10^6	60	70	<40*	-100*
10^7	60	70	<40*	>100*
10^8	60	70	<40*	>100*

*Spectral data used in conjunction with I-P plot

The effect of radiation on the threshold current differed significantly between the two types of samples. I_{th} of samples 1 and 2 did not change noticeably with irradiation, whereas samples 66 and 68 reacted in accordance with the predictions of Section VI. Possible explanations for the observed results are included in the next subsection.

MEASURED EFFECT OF RADIATION ON POWER OUTPUT

For comparison with the measured preirradiation output shown in Table 4, the output as a function of dosage at constant current is presented in Table 9.

TABLE 9. POSTIRRADIATION POWER OUTPUT AT SPECIFIC FORWARD CURRENTS

Sample	P (mW) at $I = 200$ mA			
Rad(SI)	1	2	66	68
0	44.2	51.2	81.1	31.3
10^4	59.9	54.8	43.6	9.7
10^5	57.6	56.7	14.0	6.2
10^6	59.9	63.7	*	4.6
10^7	55.1	49.6	14.0	3.5
10^8	52.8	57.6	14.2	3.8

*Uncertain data point.

While the data for samples 1 and 2 is representative of the I-P relationship over the range of I , this is not the case for samples 66 and 68. The data in Table 9 show the increase in output for samples 1 and 2 to 10^6 rad(SI) and the drastic decrease in the case of samples 66 and 68.

Theoretical considerations showed the possibility of comparative radiation hardness, but none of the principles advanced can explain the observed performance increase of samples 1 and 2. A device containing radiative recombination centers in the space charge region, a step doping profile, and heavy doping would be expected to be quite radiation resistant. Radiative recombination in the space charge region is quite resistant to irradiation; a step profile reduces n to zero in the equations relating power to dosage; and the effect of any introduced nonradiative centers would be comparatively minor at moderate dosage if, in the preirradiated device, the number of radiative centers were much larger than the number of nonradiative centers. A possible explanation for the increase in power output is that some of the radiation induced defects act as radiative recombination centers in the LCW-10 diode. This effect has not been noticed in GaAs lasers, but has been observed in SiC light-emitting diodes (Ref. 23).

The rapid drop in performance of samples 66 and 68 may possibly be attributed to device construction. Rapid deterioration would occur if the device was only lightly doped so that the introduction of nonradiative centers would have a relatively large effect. Also, higher sensitivity to radiation is predicted by the theory for a diffusion controlled output and a linear radiative center profile ($n = 1$). If the concept of the luminescent killer center is added to the above factors, the rapid degradation of samples 66 and 68 is explained.

The lack of change in the threshold current of the type LCW-10 diode samples verifies the assumption that any introduction of nonradiative recombination centers is offset. The behavior of the threshold current in the type C30127 diode samples generally adheres to the theory presented. For both samples of this type the output decreased rapidly with dosage and flat I-P curves resulted.

The data of Table 9 do not reflect losses incurred due to the walls of the dewar, nor are they corrected for the small amount of radiation missing the detector head input plane. The experimental configuration was such that any radiation within a $\sim 114^\circ$ cone would hit the detector. Equipment allowed for an error of ± 6 percent. Fixed losses as presented by the dewar were not considered important since the interest was on radiation induced changes rather than on absolute values.

POWER OUTPUT-VOLTAGE, CURRENT-VOLTAGE, AND DAMAGE FACTORS

Output versus voltage plots are presented for all samples, combining the preirradiation curve with the curve after 10^8 rad(Si). Simultaneously shown are the preirradiation and 10^8 rad(Si) current-voltage curves. Examination of Figures 23 through 26 reveals that the I-V characteristics of all samples are relatively unaffected by irradiation, showing only a slight shift to higher voltage for constant current. The effect on the P-V curves is more dramatic, and as expected, differs significantly between the two types of diodes. Type LCW-10, shown in Figures 23 and 24, exhibits a moderate decrease in output at lower voltages, where a portion of the radiative current may be attributed to a diffusion mechanism. At higher voltages it appears that an SCR mechanism becomes dominant, since the output remains relatively unaffected by irradiation.

The behavior of type C30127 diodes (Figures 25 and 26) is quite different. The large decrease in output over the whole voltage range measured indicates that a diffusion mechanism remains dominant. A possible explanation for this behavior may be the relative absence of radiative recombination centers in the space charge region. The bending of the P-V curves at higher values of V may be at least partially attributed to increasing resistive losses, although in the case of type LCW-10 diodes the changing radiative current mechanism has an effect.

Since spectra were obtained at constant current, a radiation induced shift in the emission peak may be explained, to some extent, by the changed I-V characteristics. At constant current, irradiation caused a slight increase in voltage. If a tunneling mechanism is responsible for some of the output, then the change in voltage would cause a shift in emission through its effect on the quasi-Fermi levels.

The data used to generate Figures 23 through 26 also allow calculation of the constant voltage and constant current damage factors. This information is presented in Figures 27a through 27d. Again, the almost exponential decrease in the case of samples 66 and 68 is evident. This behavior reinforces the concept of the luminescent killer center which removes a number of radiative centers from the radiative process. Values of $\tau_0 K$ have been calculated and are presented in Table 10.

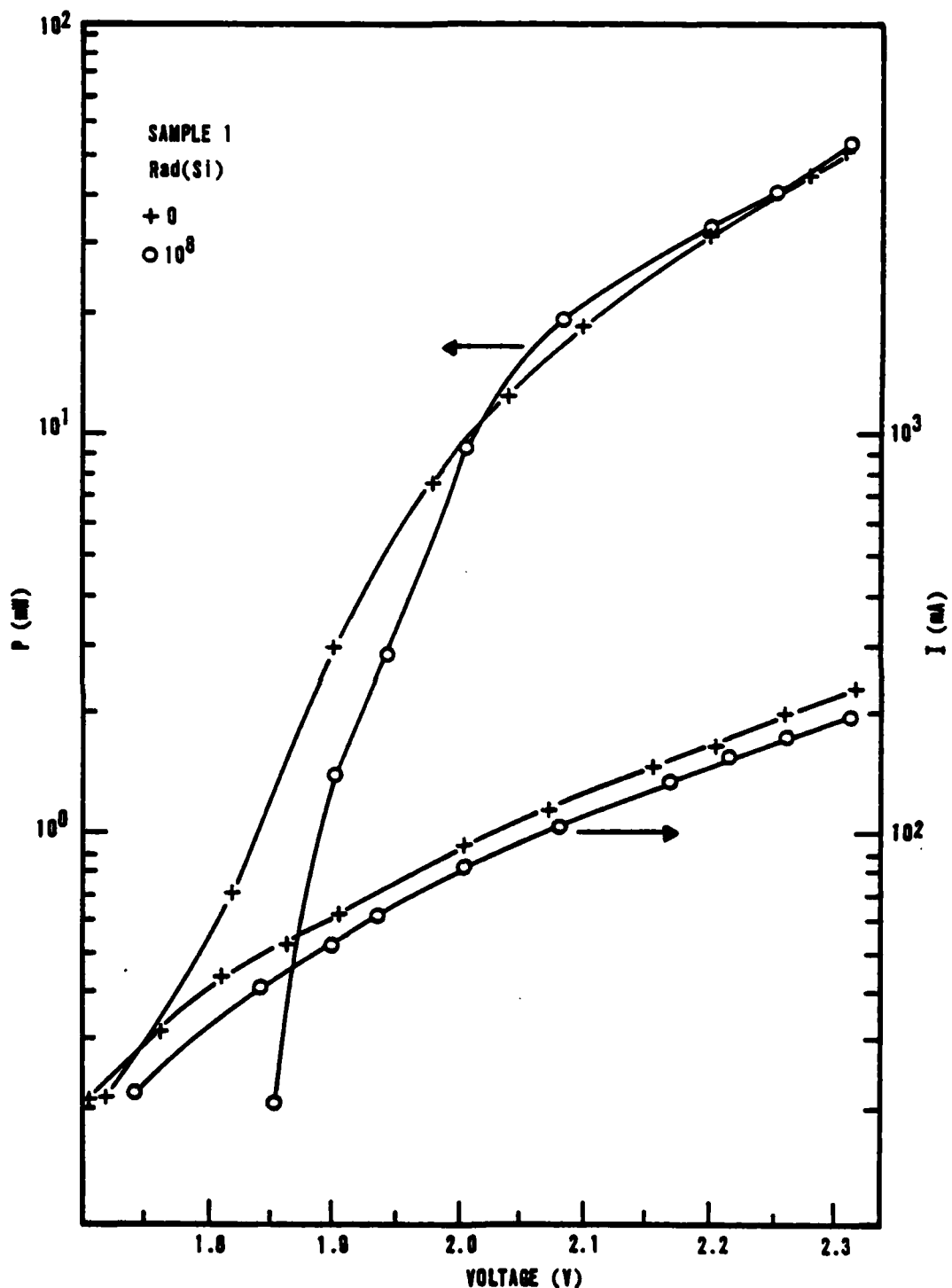


Figure 23. Power-voltage and current-voltage relation at 77 K, pre- and postirradiation.

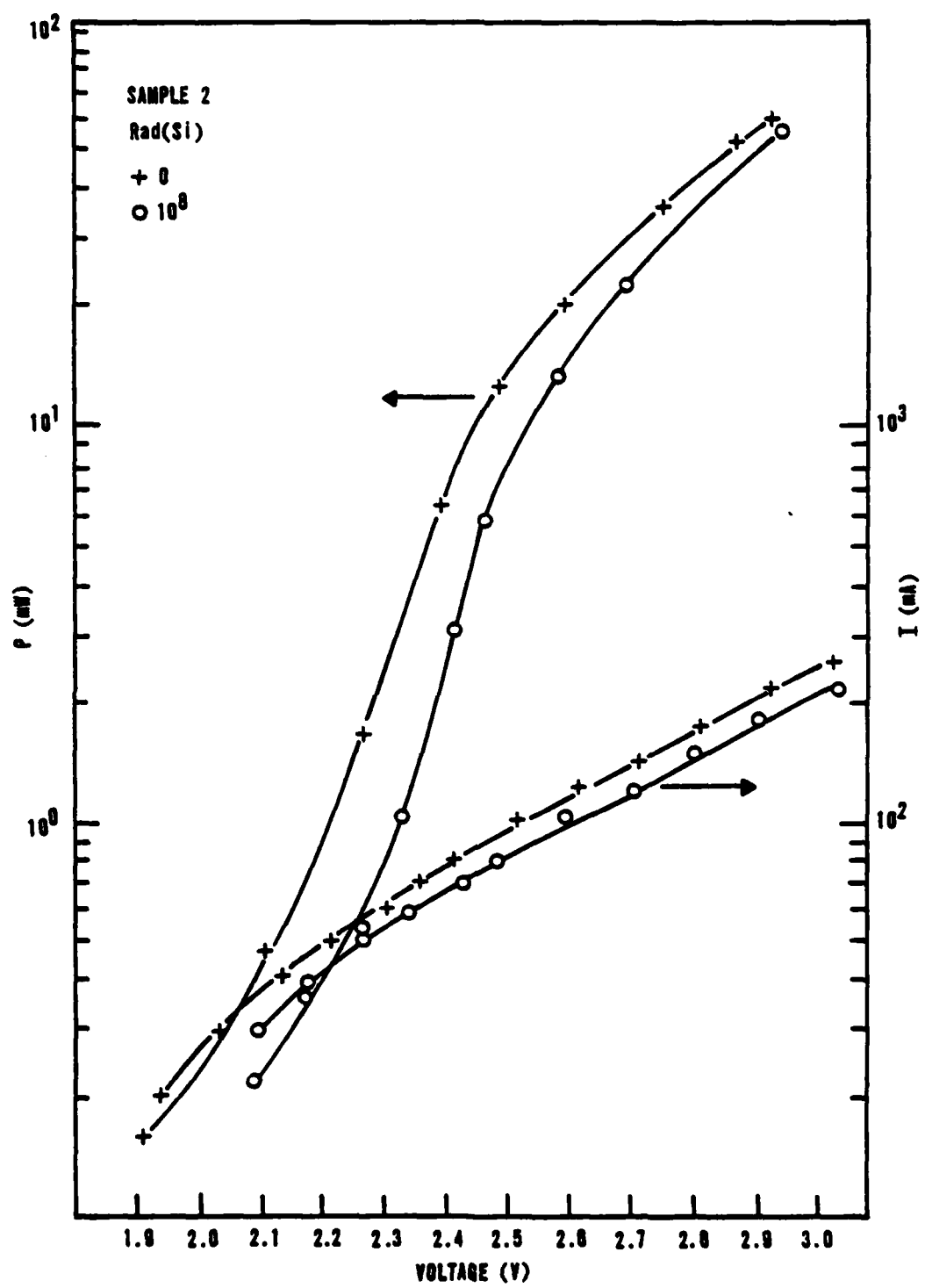


Figure 24. Power-voltage and current-voltage relation at 77 K, pre- and postirradiation.

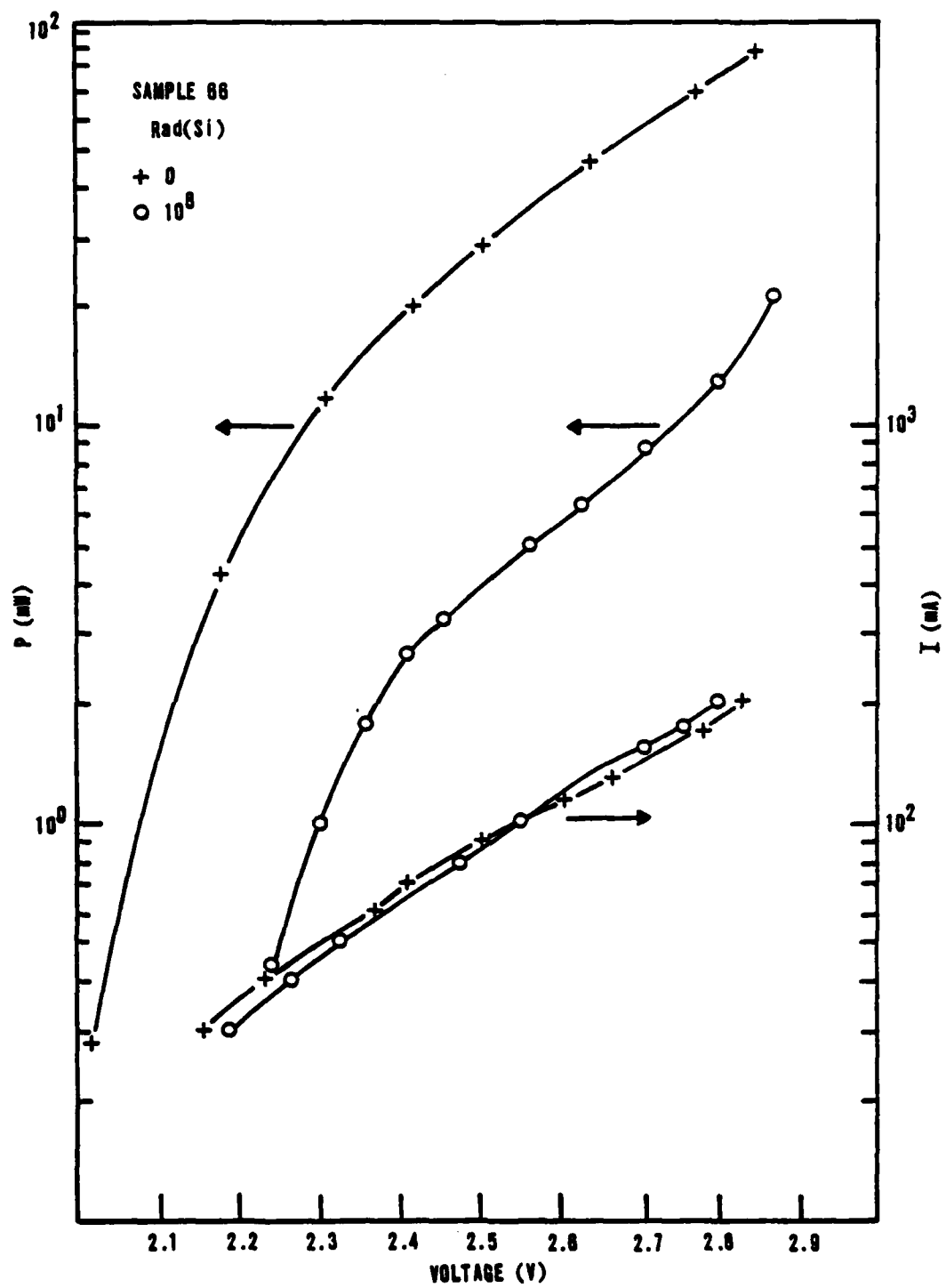


Figure 25. Power-voltage and current-voltage relation at 77 K, pre- and postirradiation.

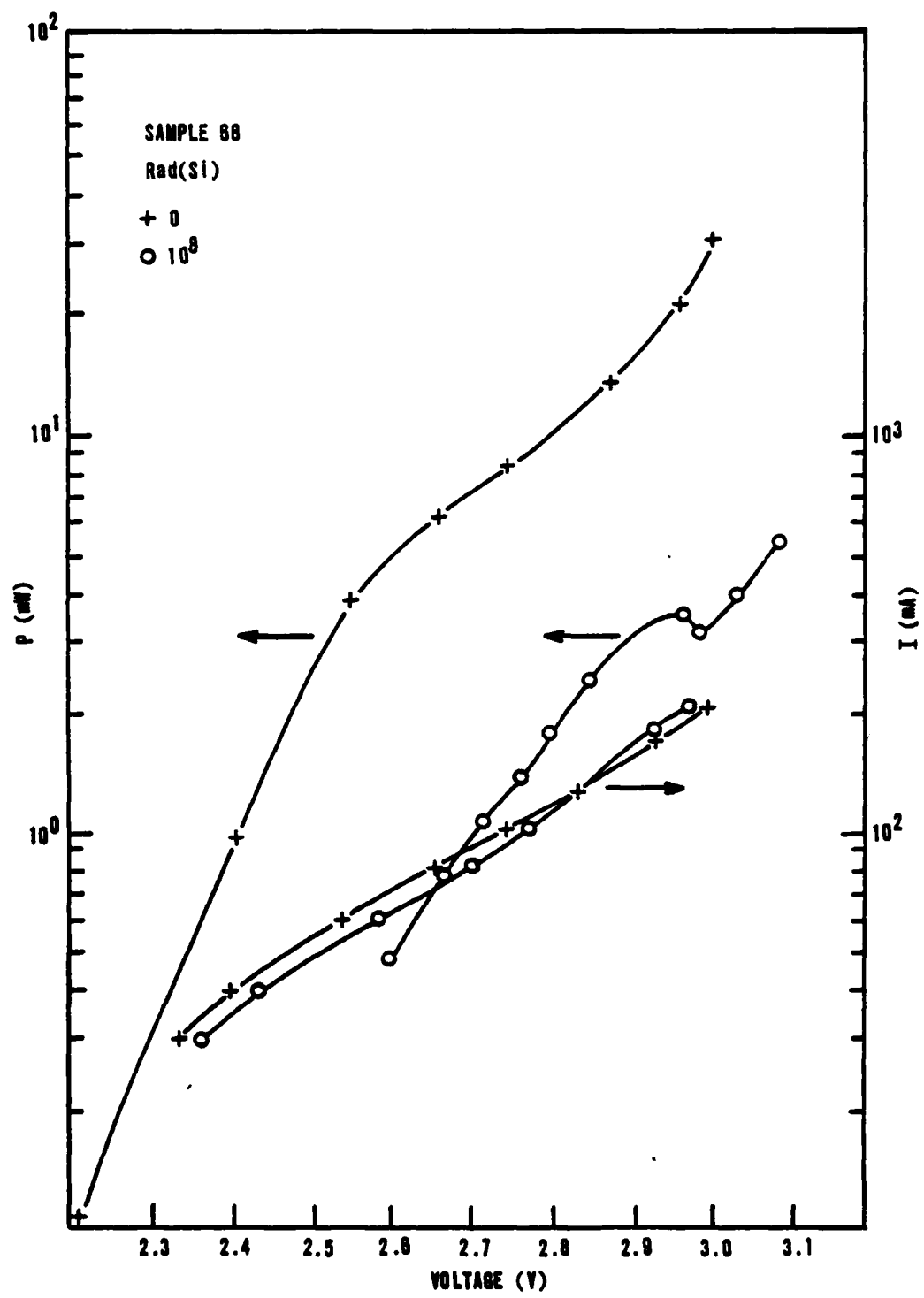


Figure 26. Power-voltage and current-voltage relation at 77 K, pre- and postirradiation.

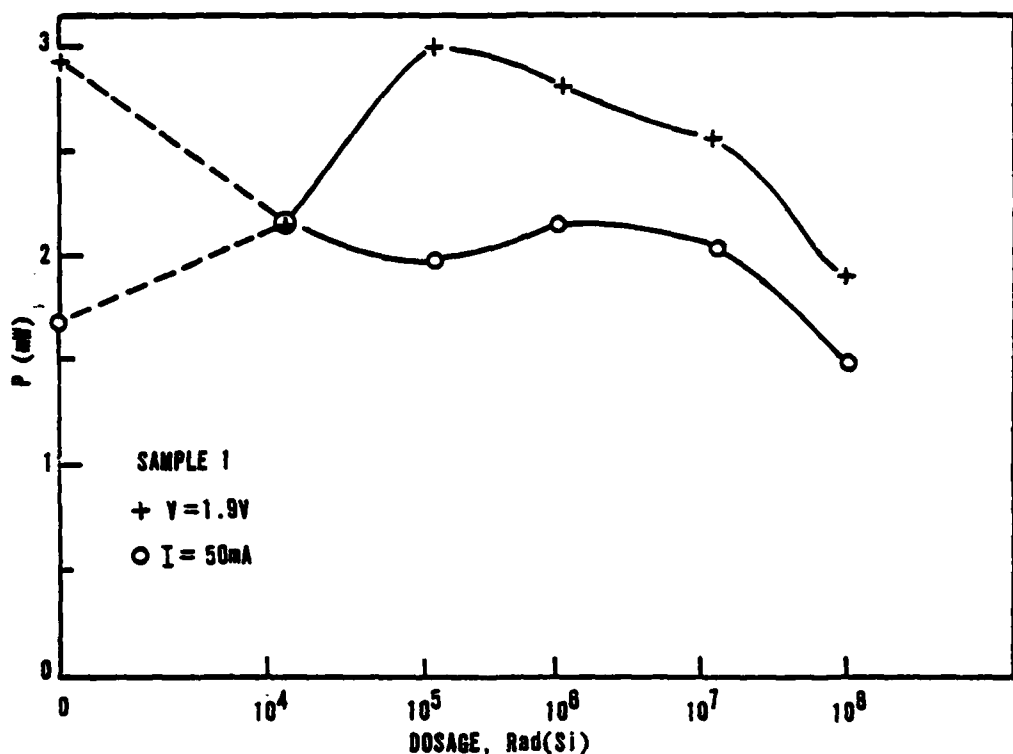


Figure 27a. Constant-voltage and constant-current change in power output at 77 K.

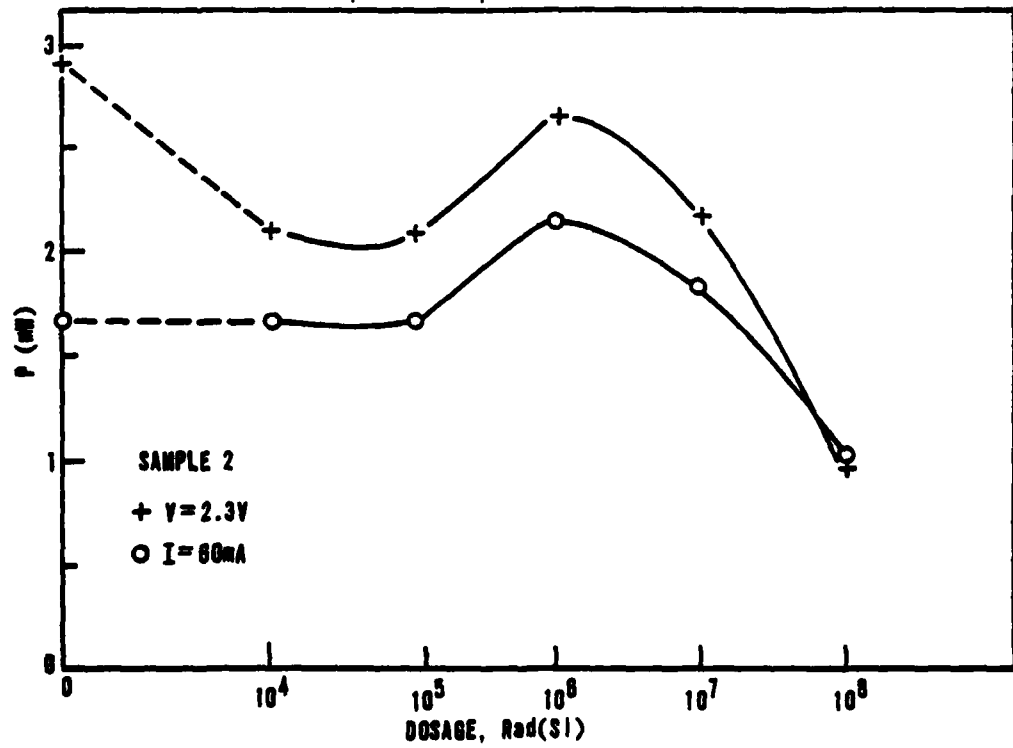


Figure 27b. Constant-voltage and constant-current change in power output at 77 K.

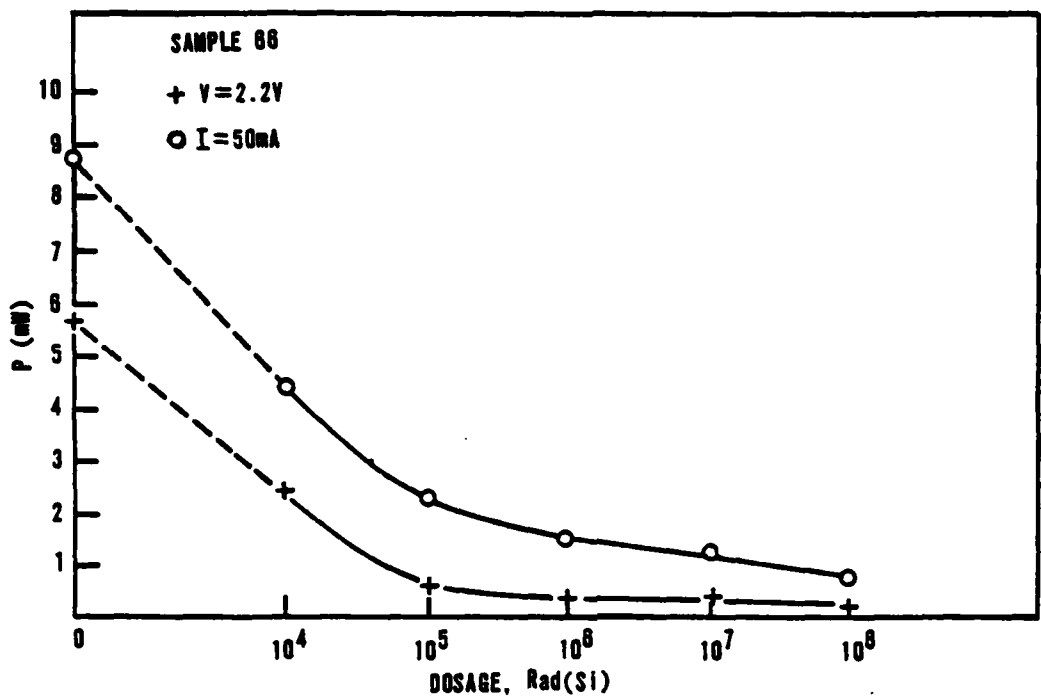


Figure 27c. Constant-voltage and constant-current change in power output at 77 K.

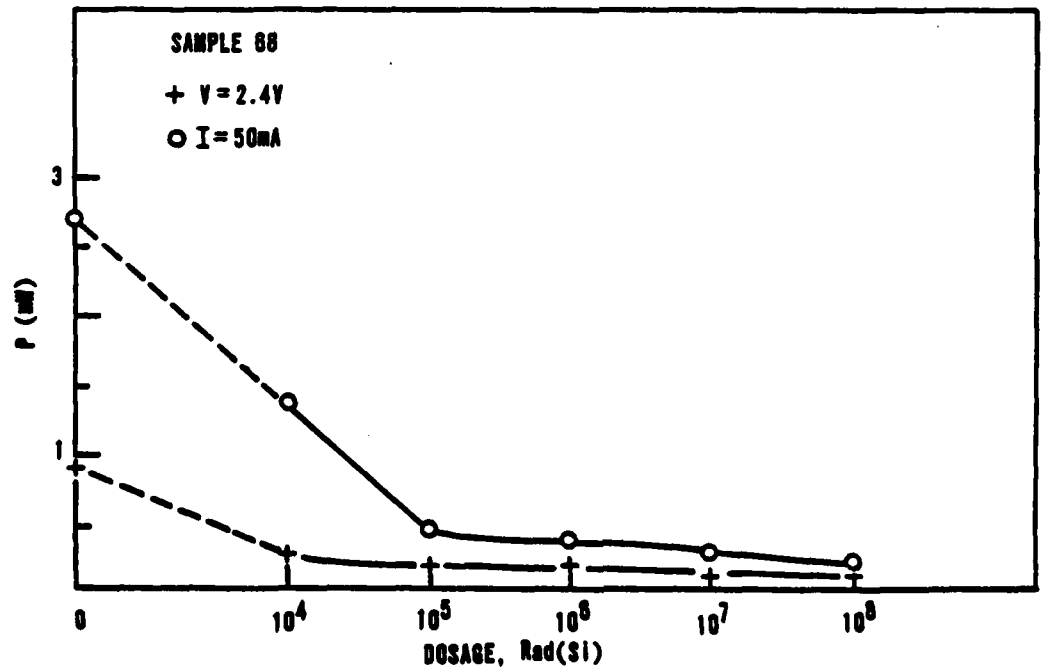


Figure 27d. Constant-voltage and constant-current change in power output at 77 K.

TABLE 10. CALCULATED DAMAGE FACTORS, $\tau_0 K$

Mechanism	Diffusion, $\tau_0 K$ (Rad $^{-1}$)		SCR, $\tau_0 K$ (Rad $^{-1}$)
Sample	Const. V	Const. I	Const. I
1	$4.4 \cdot 10^{-8}$	$1.3 \cdot 10^{-9}$	*
2	$4.3 \cdot 10^{-8}$	$2.9 \cdot 10^{-9}$	*
66	$1.2 \cdot 10^{-7}$	$3.3 \cdot 10^{-8}$	$7.9 \cdot 10^{-9}$
68	$1.6 \cdot 10^{-7}$	$4.9 \cdot 10^{-8}$	$1.0 \cdot 10^{-8}$

*At current considered, postirradiation output exceeded preirradiation output.

Since type LCW-10 diodes showed excellent radiation resistance, it was assumed for $\tau_0 K$ calculations that the radiative center profile was abrupt, or $n = 0$. For type C30127 diodes, the assumption was a linear profile, or $n = 1$. Based on the slopes of the output curves and the change in these curves with irradiation, a voltage value and a current value were selected where the radiative current appeared diffusion controlled in one case, and another set of values where the radiative current appeared to be due to SCR. Selection of these points was easily done for type LCW-10 diodes by examining Figures 23 and 24. Including a $\tau_0 K$ value based on a radiative SCR mechanism for type C30127 diodes was mainly for illustrative purposes, since Figures 25 and 26 do not indicate, considering radiation effects, a region where the output is SCR controlled.

As expected, the damage factors for type LCW-10 diodes were smaller by an order of magnitude than those obtained for type C30127 diodes. The difference in radiation sensitivity may be attributed to the factors discussed earlier.

EFFICIENCY

Radiation induced defects should have a direct effect on the efficiency of the device. Thus, if nonradiative recombination centers are introduced as a result of irradiation, the power efficiency, as well as the external differential quantum efficiency, is expected to decrease. Conversely, if the radiation induced defects act as radiative recombination centers, as proposed for type LCW-10 diodes, then an increase in efficiencies is expected. If, as has been suggested for type C30127 diodes, luminescent killer centers are introduced,

then the decrease in efficiency should be dramatic. Power efficiency at various dosages is presented in Figures 28a through 28d.

Examination of Figures 28a and 28b shows an increase in power efficiency to a dosage of 10^6 rad(Si). This is in accordance with the proposed introduction of radiative recombination center defects. Figures 28c and 28d show the rapid decline expected for a diffusion controlled output, light doping, and the possible introduction of luminescent killer centers.

EMISSION PEAK SHIFT

The wavelength at the emission peak is presented in Table 11 as a function of dosage.

The emission peak was determined by examining spectral plots. The spectral plots were surrounded by an envelope and the highest point was chosen. This method does not provide absolute information since it depends to a great extent on which mode was dominant at the time of the measurement. However, it does illustrate a general shift to higher energies. At higher dosages the spectra for samples 66 and 68 were the result of spontaneous emission rather than stimulated emission, and consequently exhibited a rather broad, flat peak.

INTENSITY DISTRIBUTION AND BEAM DIVERGENCE

The intensity distribution was measured for all samples prior to irradiation, and after 10^6 rad(Si) for samples 1 and 2 and 5×10^5 rad(Si) for samples 66 and 68. In view of the radiation resistance exhibited by the type LCW-10 diodes, no effect on the intensity distribution was expected for a dosage of 10^6 rad(Si). The measurements verified this expectation as illustrated in Figures 29 and 30. The effect of radiation on type C30127 diodes was so pronounced in all respects that the drastic change in intensity distribution, as illustrated in Figures 31 and 32, was not entirely surprising. A possible explanation may be that the radiation changed the configuration of the active region by introducing a large number of nonradiative centers, which in turn decreased the region where gain was high enough for lasing to occur. The beam divergence is presented in Table 12 and supports the idea of a changed active region for the type C30127 diodes.

For the perpendicular spread in samples 1 and 2, the single slit diffraction approximation breaks down. With that exception, good agreement exists between calculated and measured preirradiation values. The proposed change in the

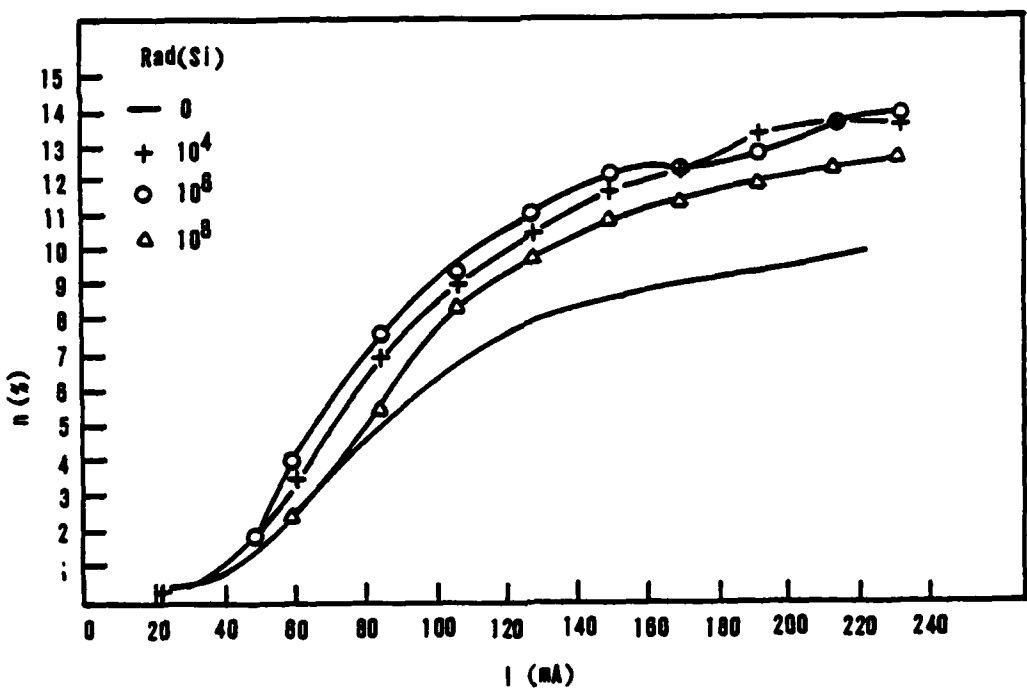


Figure 28a. Power efficiency at 77 K for selected dosages, sample 1.

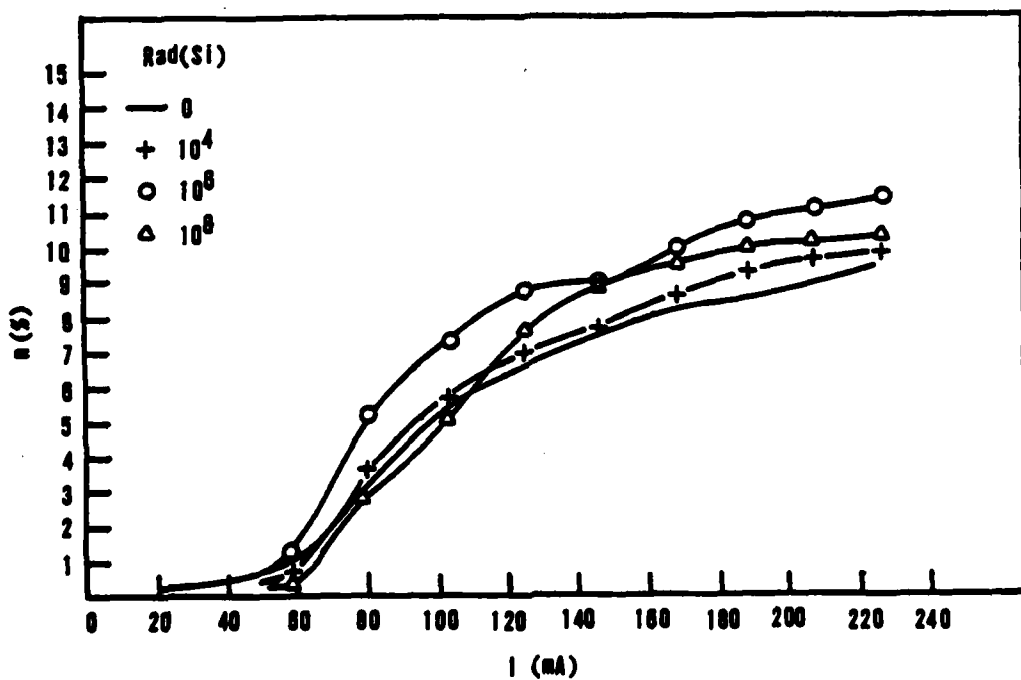


Figure 28b. Power efficiency at 77 K for selected dosages, sample 2.

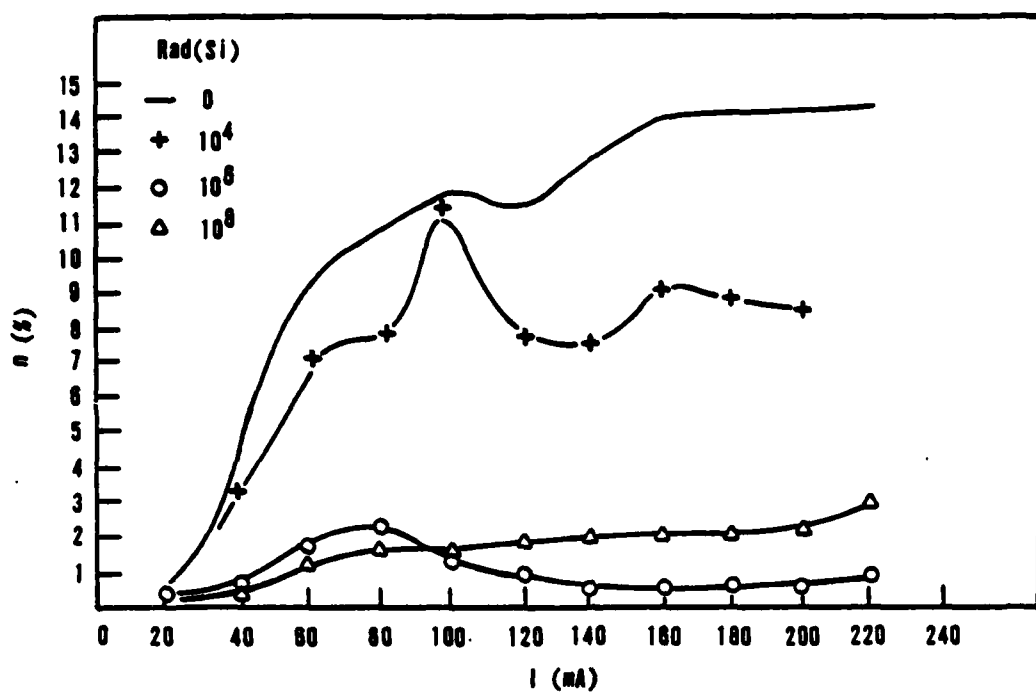


Figure 28c. Power efficiency at 77 K for selected dosages, sample 66.

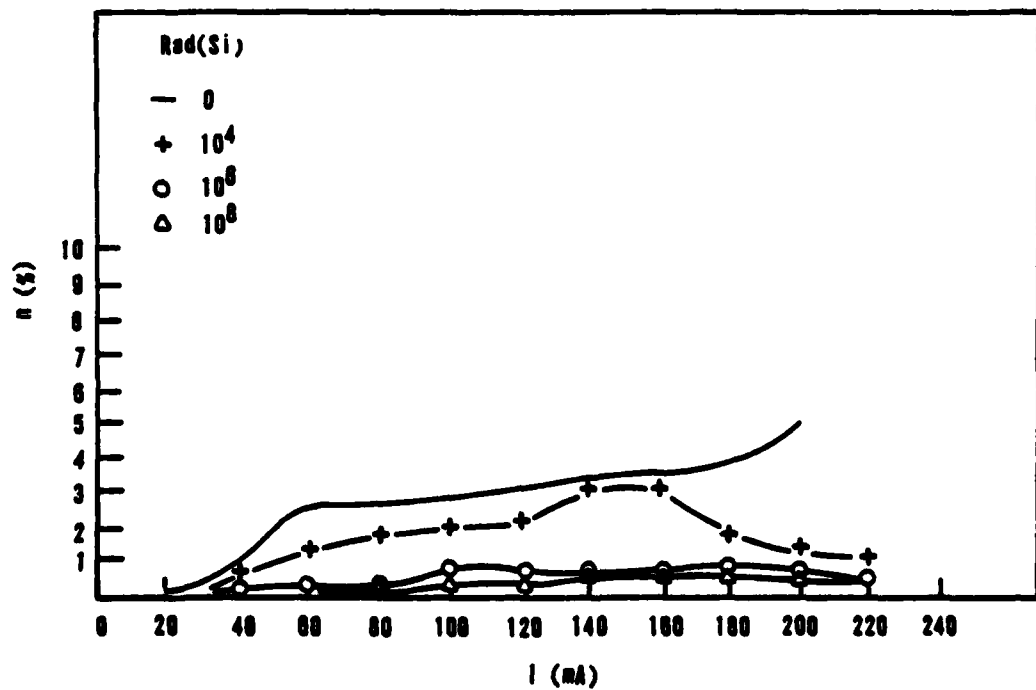


Figure 28d. Power efficiency at 77 K for selected dosages, sample 68.

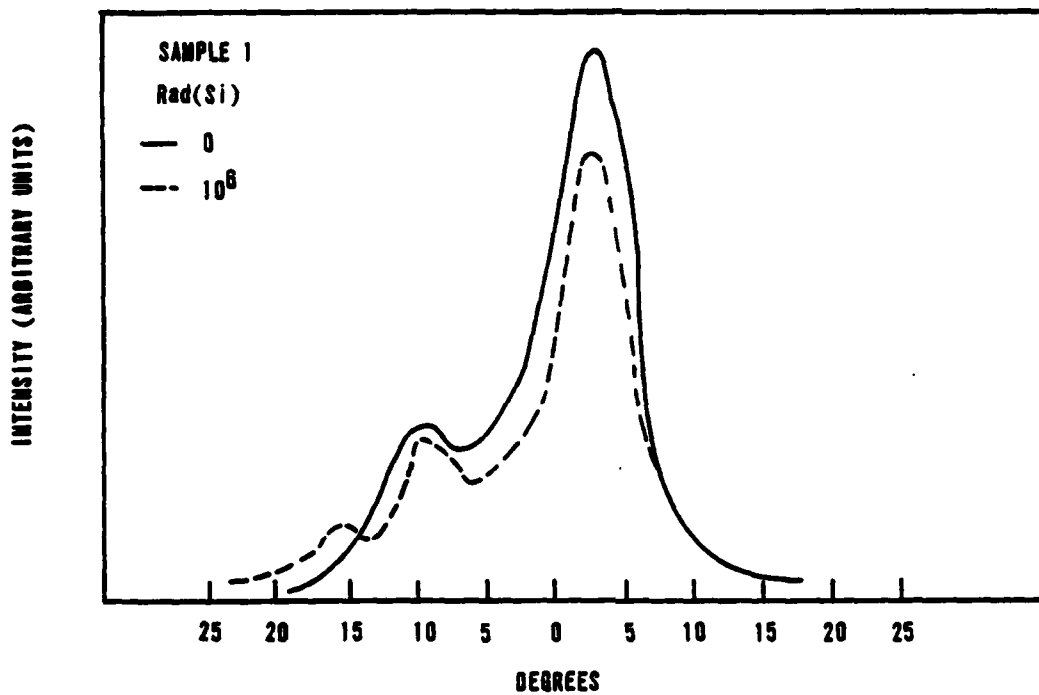


Figure 29a. Intensity distribution in far field, pre- and postirradiation, parallel to junction.

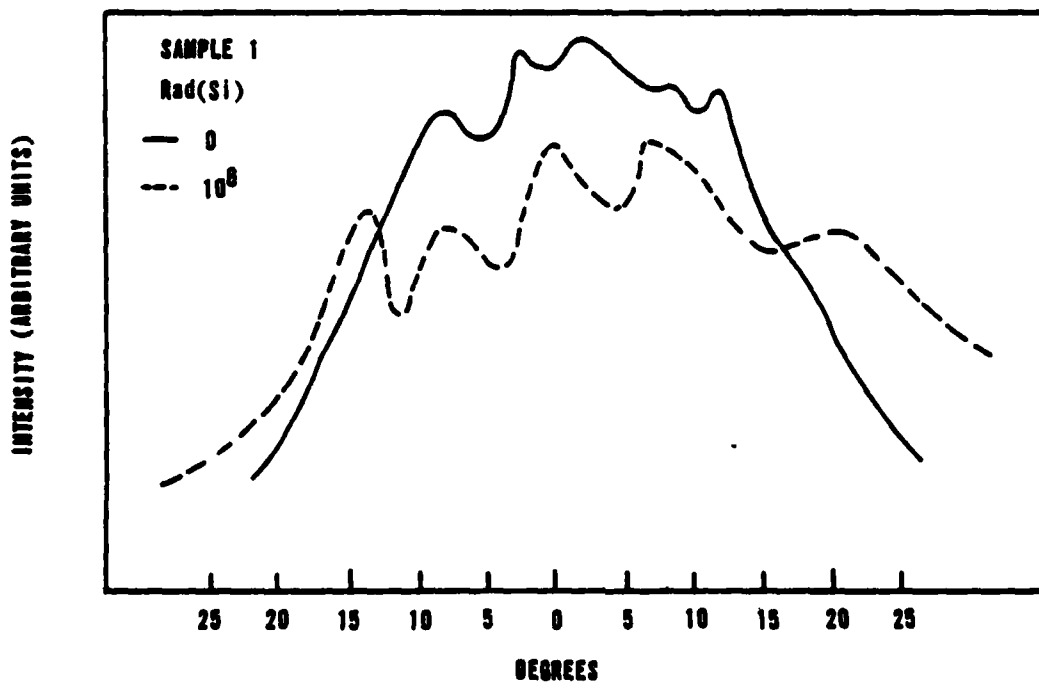


Figure 29b. Intensity distribution in far field, pre- and postirradiation, perpendicular to junction.

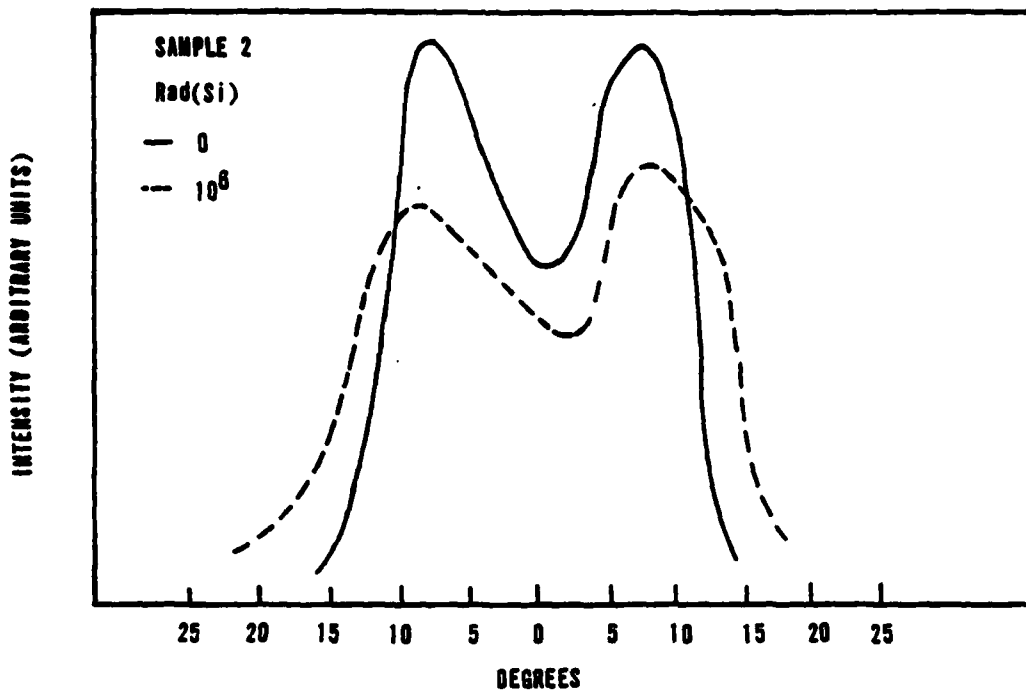


Figure 30a. Intensity distribution in far field, pre- and postirradiation, parallel to junction.

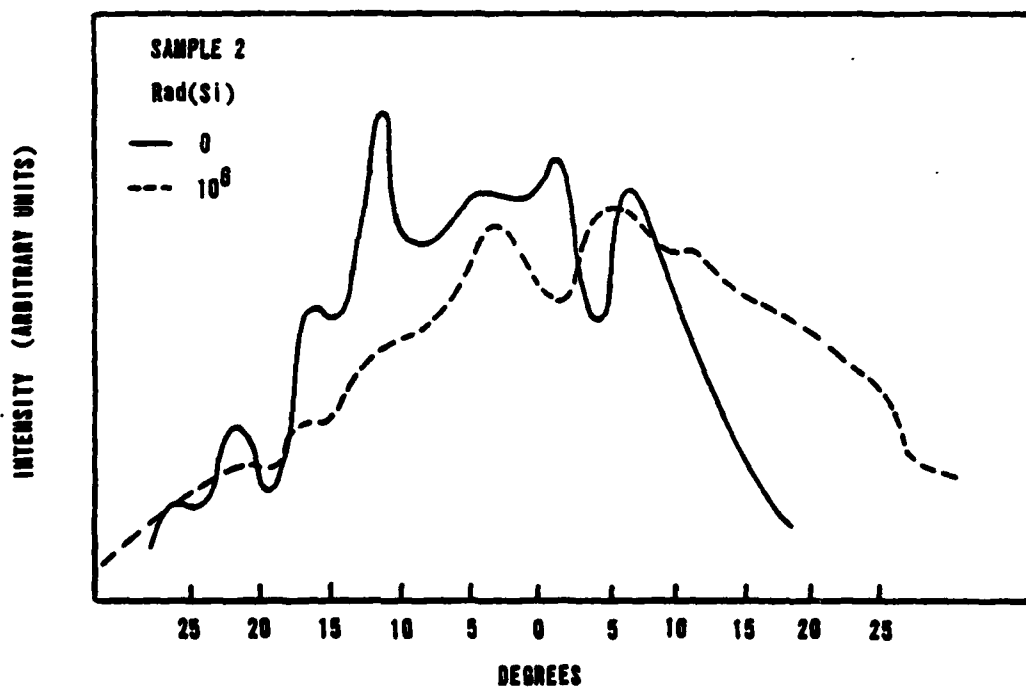


Figure 30b. Intensity distribution in far field, pre- and postirradiation, perpendicular to junction.

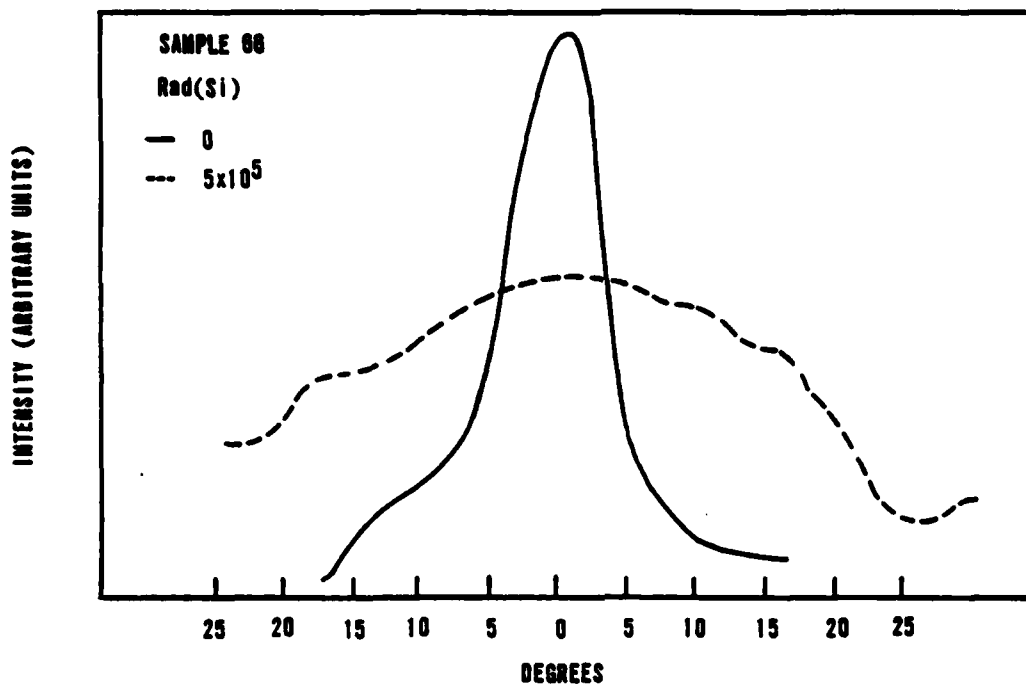


Figure 31a. Intensity distribution in far field, pre- and postirradiation, parallel to junction.

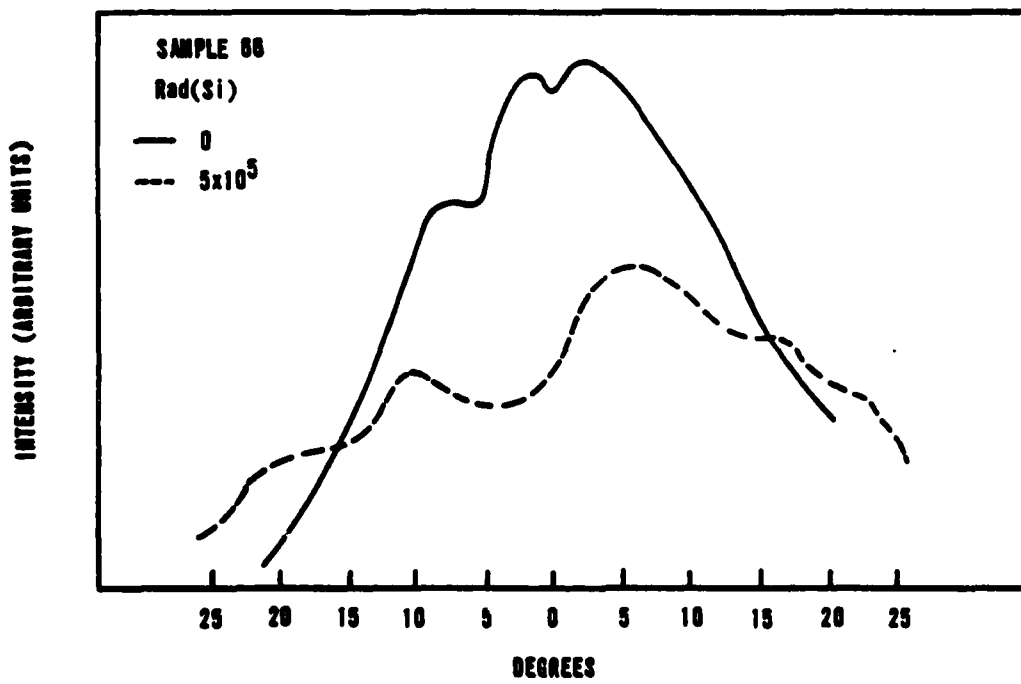


Figure 31b. Intensity distribution in far field, pre- and postirradiation, perpendicular to junction.

INTENSITY (ARBITRARY UNITS)

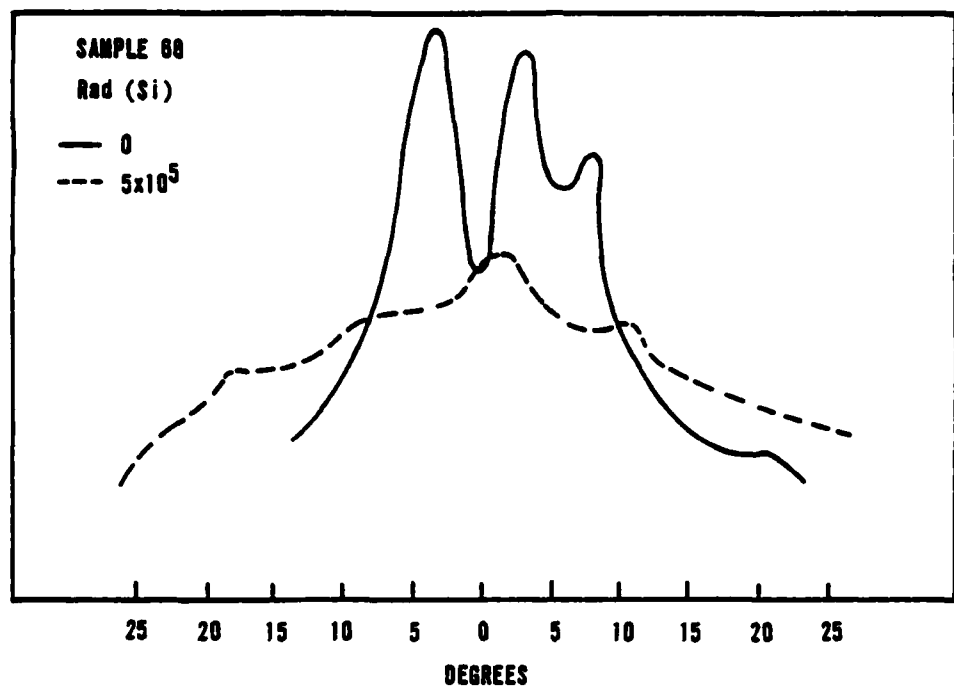


Figure 32a. Intensity distribution in far field, pre- and postirradiation, parallel to junction.

INTENSITY (ARBITRARY UNITS)

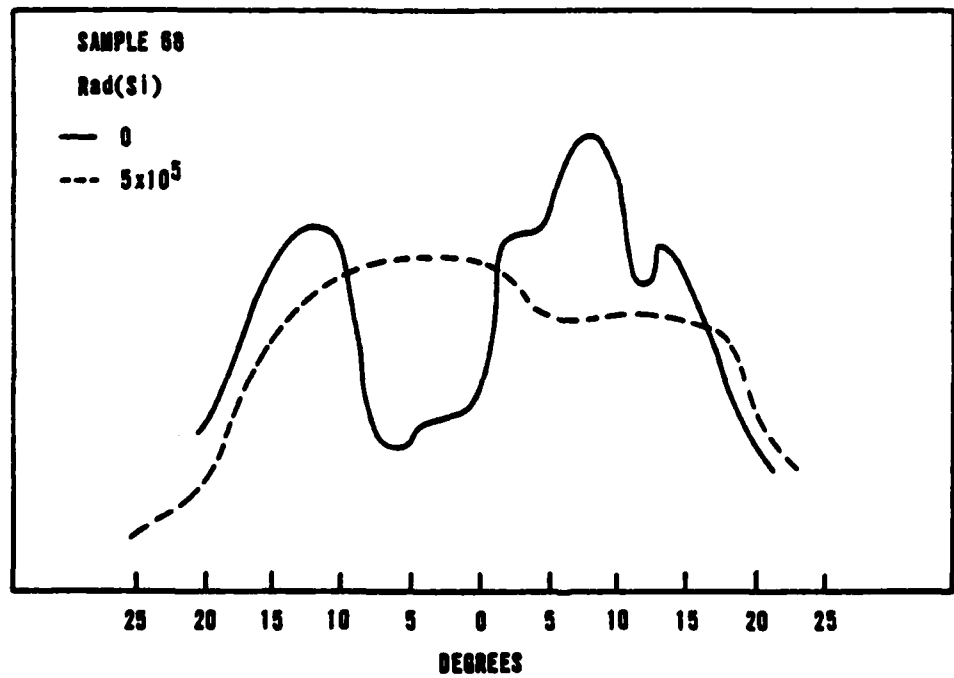


Figure 32b. Intensity distribution in far field, pre- and postirradiation, perpendicular to junction.

TABLE 11. EMISSION PEAK MEASURED AT CONSTANT CURRENT AS A FUNCTION OF DOSAGE

Sample Rad(Si)	Emission Peak (nm)			
	1	2	66	68
10	829.2	839.5	764.7	768.3
10^4	828.6	839.9	763.5	767.3
10^5	829.2	839.5	762.7	767.6
10^6	829.2	839.5	762.1	767.1
10^7	829.5	839.5	762.3	767.1
10^8	828.1	839.0	762.3	767.6

TABLE 12. BEAM DIVERGENCE BEFORE AND AFTER IRRADIATION

Sample*	Beam Divergence (degrees, HWHM)		
	Calculated	Preirradiation	Postirradiation**
1	4	3	3
	—	22	19
2	4	12	11
	—	19	16
66	4	4	19
	—	17	19
68	4	10	23
	—	26	18

*|| and — indicate parallel and perpendicular to the junction plane, respectively

** 10^6 rad(Si) for samples 1 and 2; 5×10^5 rad(Si) for samples 66 and 68

extent of the active region falls in line with the measured postirradiation values. The introduction of additional radiative centers could widen the region and thus result in less beam divergence, as appears to have happened for the spread in samples 1 and 2. Conversely, the severe reduction of radiative centers in samples 66 and 68 could reduce the active region and result in large values of divergence. According to the measured values, using the narrow slit approximation, the width of the active region in samples 66 and 68 was reduced to a value near the thickness, so that the light, instead of being emitted by a narrow slit, is actually being emitted by a small rectangular aperture.

IX. CONCLUSIONS

The primary conclusion is that the LCW-10 injection lasers are much more resistant to irradiation by a gamma source than the C30127 injection lasers.

The LCW-10 lasers exhibited increased light output to 10^6 rad(Si) and at 10^8 rad(Si) still performed comparably with preirradiation values. The threshold current value did not noticeably change as a result of irradiation, nor were the intensity distribution and beam divergence significantly affected. The LCW-10 laser's power and external differential quantum efficiency also increased initially.

The C30127 laser's performance degraded rapidly in all respects. Light output decreased by half after only 10^4 rad(Si), threshold current increased, efficiencies decreased, and beam characteristics changed drastically.

Without knowledge of device composition and structure, some assumptions were made. The calculated damage factors show that these assumptions are probably valid. It is believed that the output of the LCW-10 laser is due to SCR while that of the C30127 laser is diffusion controlled. Additionally, it is thought that the former was heavily doped while the latter was only lightly doped.

The quantitative results given throughout this study are believed to accurately represent radiation-induced performance changes in both of the injection lasers. Since the investigation was concerned only with the two specific types, the results apply only to them, and even then should be used with care since only two samples of each type were tested.

X. RECOMMENDATIONS

The data obtained in this study are of necessity quantitative only. Interpretation of experimental results had to be largely based on assumptions about device composition. In view of this, it was not possible to assign a specific result to a definite physical process or mechanism.

If detailed information could be obtained from the respective manufacturers, a physical interpretation of the results may be possible. This information, in turn, could possibly serve to create devices of even greater radiation hardness than the present type LCW-10 laser. Additionally, the effects of radiation other than gamma should be investigated, since results could differ considerably.

Another area to be investigated concerns the annealing behavior, either due to forward bias or elevated temperatures. This could provide further insight into the physical processes occurring within each device.

REFERENCES

1. Rediker, R. H., "Semiconductor Lasers," Physics Today, 18, pp 42-50, 1965.
2. Kressel, H., "Semiconduction Lasers," Lasers, 3, Marcel Dekker, Inc, New York, 1971.
3. Hayashi, I., et al., "Junction Lasers Which Operate Continuously at Room Temperature," Applied Physics Letters, 17, pp 109-111, 1970.
4. Aukerman, L. W., et al., "Radiation Effects in GaAs," J. Appl. Phys., 34, pp 3590-3599, 1963.
5. Barnes, C. E., "Neutron Damage in GaAs Laser Diodes: At and Above Laser Threshold," IEEE, NS-19, pp 382-385, 1972.
6. Fast Neutron Effects on Diffused Gallium Arsenide Lasers, AFWL-TR-73-23, Air Force Weapons Laboratory, Kirtland Air Force Base, N. Mex., 1973.
7. Saji, M. and Inuishi, Y., "Radiation Damage and Annealing of GaAs Laser Diode," Japan. J. Appl. Phys., 4, pp 830-831, 1965.
8. Compton, D. M. J. and Cesena, R. A., "Mechanisms of Radiation Effects on Lasers," IEEE, NS14-6, pp 55-61, 1967.
9. Barnes, C. E., "Effects of Co⁶⁰ Gamma Irradiation in Epitaxial GaAs Laser Diodes," Physical Review, 1-12, pp 4735-4747, 1970.
10. Share, S., et al., "Properties of Compensated GaAs Light-Emitting Diodes Following Co⁶⁰ Irradiation," Solid State Electronics, 18, pp 471-480, 1975.
11. Sze, S. M., Physics of Semiconductor Devices, Wiley-Interscience, New York, 1969.
12. Kressel, H. and Ladany, I., "Reliability Aspects and Facet Damage in High-Power Emission from (AlGa)As CW Laser Diodes at Room Temperature," RCA Review, 36, pp 230-239, 1975.
13. O'Shea, D. C., et al., A Laser Textbook, Georgia Institute of Technology, 1975.
14. Barnes, C. E., "Neutron Damage in Epitaxial GaAs Laser Diodes," J. Appl. Phys., 42, pp 1941-1949, 1971.
15. Grill, R. B., et al., Injection Laser Sources for Fiber Optic Communications, Laser Diode Labs, Inc, Metuchen, New Jersey.
16. Lederer, M. C., et al., Table of Isotopes (Sixth Edition), John Wiley and Sons, New York, 1967.
17. Campos, M. D., et al., "Cavity Competition in Anomalous Emission Intensity in Double-Heterostructure (DH) Lasers," IEEE, QE-13, pp 687-691, 1977.
18. Kobayashi, K., "Unstable Horizontal Transverse Modes and Their Stabilization with a New Stripe Structure," IEEE, QE-13, pp 659-661, 1977.

REFERENCES (CONTINUED)

19. Risch, C. H., et al., "External-Cavity-Induced Nonlinearities in the Light Versus Current Characteristics of (GaAl)As Continuous Wave Diode Lasers," IEEE, QE 13, pp 692-696, 1977.
20. Lambert, K. P., et al., "A Comparison of the Radiation Damage of Electronic Components Irradiated in Different Radiation Fields," Nuclear Instruments and Methods, 130, pp 291-300, 1975.
21. Aukerman, L. W., et al., "Effects of Radiation Damage on the Behavior of GaAs p-n Junctions," IEEE, NS13-6, pp 174-180, 1966.
22. Pankove, J. I., Optical Processes in Semiconductors, Dover Publications, Inc, New York, 1975.
23. Stanley, A. G., "Comparison of Light-Emitting Diodes in a Space Radiation Environment," IEEE, NS17-6, p 239, 1970.